Macromolecular Crowding Effects on Cellular NADH-enzyme Binding Kinetics

A THESIS
SUBMITTED TO THE FACULTY OF THE
UNIVERSITY OF MINNESOTA
BY

Shane Wilson

IN PARTIAL FULFILLMENT OF THE REQUIREMENTS
FOR THE DEGREE OF
MASTER OF SCIENCE

Dr. Ahmed A. Heikal

August 2017

Acknowledgements

I would first like to acknowledge the assistance of my advisor, Dr. Heikal. Thank you for always being so kind throughout my whole graduate experience. When things seems to be piling up and become stressful, you make everything feel manageable.

Tylor Franklin, thank you for all your help with this project. Your work ethic as an undergraduate was inspiring, and I wish you the best with your post-graduation plans.

Megan Currie, you joined the lab before all of us and you passed on all your knowledge and experience without hesitation. We all really appreciate your help. Congratulations on being done!

Dr. Holy, thank you for sacrificing your time to train me on cell culture. I owe my successful cell studies and results to you. They would not have been completed without your help and input.

To everyone in the Heikal/Sheets group: Thank you for all your kind feedback on my research and always asking engaging questions

I would like to acknowledge the assistance of my thesis committee members, Dr. Berry, Dr. Clarke, Dr. Siders, and the relationships that have been fostered through this experience. Your feedback, encouragement, and time have been treasured.

Fellow graduate students, I wish you the best with all your future endeavors. I could not have asked for a better group of people to spend these past two years with.

Dedication

This thesis is dedicated to my father and mother for their continuous encouragement.

Abstract

Reduced nicotinamide adenine dinucleotide (NADH) is a major cofactor for a large number of biological enzymes that are essential in a myriad of metabolic pathways such as glycolytic and oxidative phosphorylation pathways. In addition, NADH is intrinsically fluorescent and therefore has the potential of serving as a biomarker to monitor mitochondrial dysfunctions associated with aging, cancer, and apoptosis. In this thesis, we investigate how macromolecular crowding may affect the biochemical reaction kinetics of NADH interaction with lactate dehydrogenase (LDH) as a model system in biomimetic crowding (e.g., Ficoll-enriched buffer at $0-400$ g/L). Using noninvasive, quantitative two-photon fluorescence lifetime and associated anisotropy, we exploit the sensitivities of NADH fluorescence lifetime and rotational diffusion to protein binding. To differentiate between viscosity and crowding effects on the reaction kinetics, we also conducted complementary measurements in glycerol-enriched buffer. Additionally, we are investigating the sensitivity of cellular NADH interaction with dehydrogenases to metabolic manipulations. Our quantitative and non-invasive methodology complements the traditional biochemical and thermodynamics techniques without the destruction of live cells. Intracellular NADH also exists as a mixture of free and enzyme-bound populations at dynamic equilibrium throughout living cells, which can be imaged using fluorescence lifetime imaging for both quantitative and noninvasive assessment of cellular metabolism. 2P-fluorescence lifetime imaging microscopy (FLIM) and 2P-fluorescence anisotropy of intrinsic NADH was measured in cultured mouse embryonic cells under both resting conditions and metabolic-manipulation.

Table of Contents

List of Tables

List of Figures

List of Abbreviations

2P-Anisotropy	Two-Photon Fluorescence Anisotropy
2P-FLIM	Two-Photon Fluorescence Lifetime Imaging Microscopy
2P-Lifetime	Two-Photon Fluorescence Lifetime
ATCC	American Type Culture Collection
ATP	Adenosine Triphosphate
C3H10	C3H10T1/2 Fibroblast Cells
Coumarin	7-hydroxycoumarin-3-carboxylic acid
cP	Centipoise
DIC	Differential Interference Contrast
DMEM	Dulbecco's Modified Eagle's Medium
DMSO	Dimethyl Sulfoxide
EDTA	Ethylenediaminetetraacetic acid
FWHM	Full Width at Half Maximum
G-Factor	Geometric Factor
LDH	L-Lactate Dehydrogenase
MCP-PMT	Microchannel Plate Photo Multiplier Tube
MitoTracker	MitoTracker Green FM
NA	Numerical Aperture
NAD+	Nicotinamide Adenine Dinucleotide, Oxidized
NADH	Nicotinamide Adenine Dinucleotide, Reduced
NADPH	Nicotinamide Adenine Dinucleotide Phosphate, Reduced
Rh123	Rhodamine 123

TCSPC	Time Correlated Single Photon Counting
Tris buffer	tris(hydroxymethyl)aminomethane
UV	Ultraviolet

List of Symbols

α_i	Amplitude fraction of the i^{th} species
$\langle \tau_{fl} \rangle$	Average fluorescence lifetime
K_B	Boltzmann constant
K_d	Dissociation constant
K_{eq}	Equilibrium Constant
$I_{54.7^\circ}$	Magic-angle Fluorescence Intensity
I_T	Total fluorescence intensity
τ_i	Fluorescence lifetime of the i^{th} species
β_i	Initial anisotropy of the i^{th} species
$I_{\|\|}$	Parallel polarized fluorescence intensity
$I_\perp$	Perpendicular polarized fluorescence intensity
r(t)	Time-resolved anisotropy
r_{ss}	Steady-state anisotropy
ϕ_i	Rotational diffusion coefficient of the i^{th} species
η	Viscosity
f_B	Fraction of enzyme-bound NADH
f_1/f_2	Population fraction of species with distinct fluorescence lifetime
t	Time
T	Temperature
γ	Enhancement factor
V	Hydrodynamic radius

G	Geometric factor

Chapter 1: Introduction

1.1 Cells are Highly Crowded

Conventional *in vitro* interactions of enzymes and coenzymes have been extensively studied,[1] and thermodynamic and kinetics data is well known for a myriad of enzymatic interactions.[1] However, such characterization of these interactions are lacking in both biomimetic environments and living cells. Unlike *in vitro* studies carried out in a buffer, a cell is highly crowded with macromolecules (up to 400 g/L) that are believed to affect cellular processes like protein folding, rates of diffusion, and enzyme binding.[1-5] Macromolecular crowding is present in all living cells due to the presence of proteins, DNA, RNA, biomembranes, and other organelles.[6] For example, the concentration of hemoglobin in a red blood cell is about 340 g/L.[7] If this was studied in a dilute, *in vitro* system, the activity of hemoglobin would be two orders of magnitude less than in a crowded environment.[7] Macromolecular crowding is often studied in solutions that are enriched in "crowding agents". These crowding agents are usually synthetic sugar polymers or proteins of a specific size, shape, and surface charge. Ideally, for the most accurate modeling of macromolecular crowding, cell extracts would also be used. However, to simplify the solutions, inert crowding agents of specific sizes and shapes will be considered to study how homogenous and heterogeneous crowding agents affect kinetics while eliminating electrostatic interactions due to surface charges. In Figure 1.1 we model the difference between these two types of crowding. In Figure 1.1 (A), a homogenously viscous environment is shown where there is no excluded volume

occupied by crowding agents, but the reactants could potentially be affected by the bulk viscosity (i.e. glycerol).[2] This viscosity effect has the potential to stabilize product formation and slow down the rotational and diffusion time of molecules according to the Stokes-Einstein model.[2] Figure 1.1 (A) and Figure 1.1 (A) are models that show heterogeneous crowded environments, rich in macromolecules. In contrast to homogeneous buffer (A), excluded volumes represented by crowding agents are obstacles standing in the way of reactants (A) and can potentially prevent product formation. However, in order to reduce steric interactions in crowded systems, product formation can be favored to reduce the macromolecular volume.[7] A cage made of those crowding agents may confine reactants in a tight place that would potentially enhance an encounter between reactants leading to product formation and an increased association constant (A).[7] With this in mind, we will explore these three models of crowding based on their effects on binding kinetics.

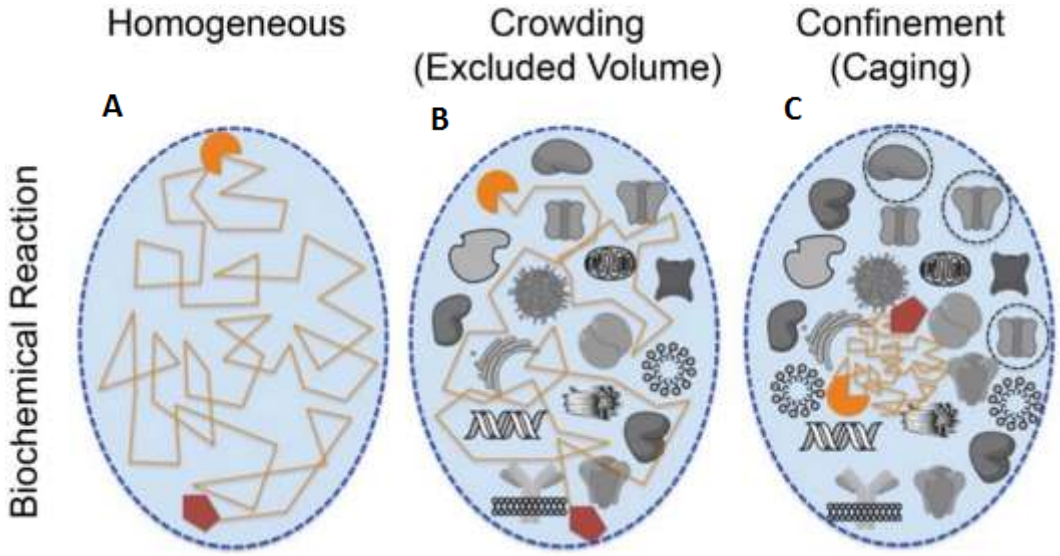

Figure 1.1: Schematic representation of potential crowding effects within solution and cells.[8]

1.2 Role of NADH

Nicotinamide adenine dinucleotide (NADH) is an intrinsic coenzyme that is involved in a wide range of redox reactions and metabolic pathways such as glycolysis and oxidative

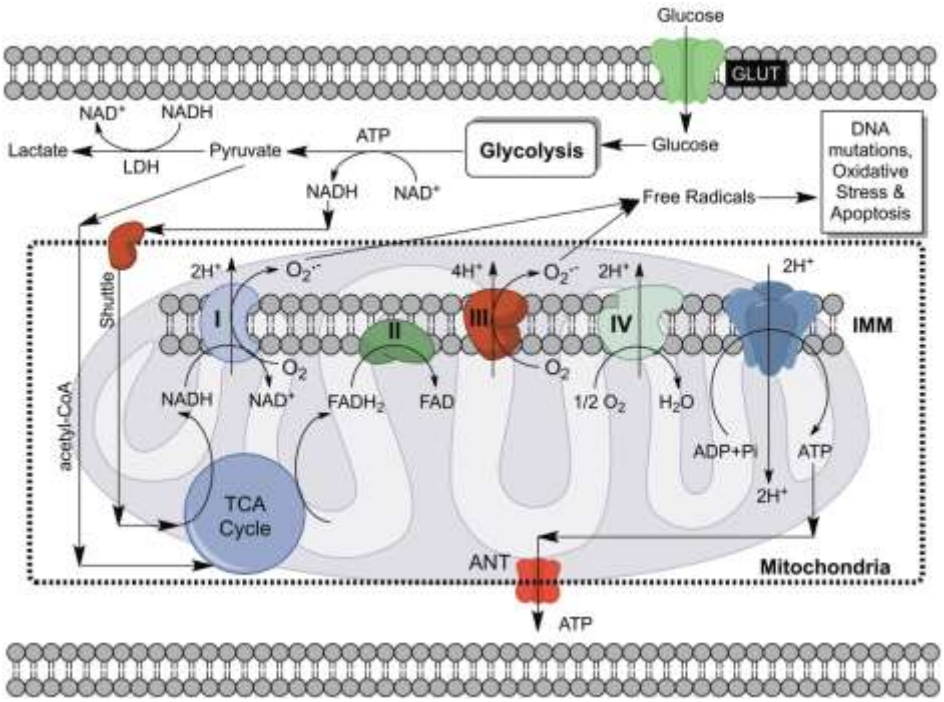

Figure 1.2: NADH is involved in energy metabolism (glycolysis and oxidative phosphorylation).

phosphorylation (Figure 1.2). [9-13] Throughout glycolysis and the citric acid cycle, oxidized nicotinamide adenine dinucleotide (NAD^+) is reduced to NADH by accepting electrons in the form of hydride. NADH is a high energy electron carrier that shuttles its electrons to protein complexes imbedded within the inner membrane of the mitochondria to ultimately make the energy currency, adenosine triphosphate (ATP). Because of its involvement in metabolism and cellular function, NADH has the potential to diagnose the physiological state of the cell.[14-15] For example, it is known that healthy cells heavily rely

on oxidative phosphorylation pathways for energy production, while cancerous cells, have been shown to shift towards glycolytic pathways.[14] This shift of priority in metabolism between healthy and cancerous cells, called the *Warburg Effect*, has been monitored through endogenous NADH.[10, 14, 16]

1.3 NADH is a Natural Fluorescent Biomarker

NADH is an intrinsic biomarker because it is naturally fluorescent, while its oxidized form (NAD^+) is not. NADH contains a nicotinamide ring (Figure 1.3), which contains conjugated double bonds that contributes to a fluorescence emission at 460 nm.[9, 17] In a cell, NADH can exist as both free NADH and enzyme-bound NADH.[18] The fluorescent lifetime of free and enzyme-bound NADH can be used to differentiate the two components. Free NADH has an average fluorescent lifetime of 0.4 ns in buffer, while enzyme-bound NADH can have a much longer lifetime that can be greater than 1.2 ns.[19]

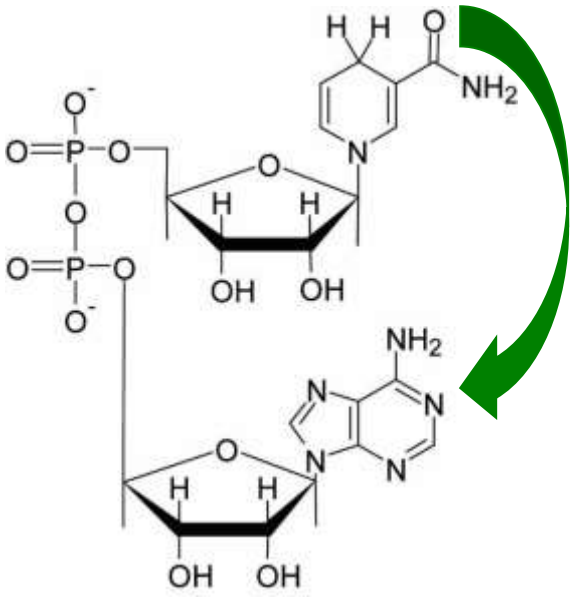

Figure 1.3: Reduced Nicotinamide adenine dinucleotide (NADH). Green arrow shows possible quenching through adenine and nicotinamide ring stacking

When NADH is bound to enzymes, a stretched conformation prevails where the nicotinamide and adenine rings remain separated, prohibiting quenching.[13, 19] In contrast, free NADH is flexible and can exist as two components (folded and stretched); this flexibility leads to a much shorter lifetime due to potential quenching. [13, 19] Figure 1.3 highlights this flexibility and potential quenching though the arrow. This difference in fluorescence lifetime can be used as a noninvasive, quantitative tool to elucidate how the ratio of enzyme-bound and free NADH is allocated within a cell under different physiological conditions. This allocation of NADH has the potential to reveal mitochondrial function or dysfunction. It is important to note that NADH and NADPH have the same spectral properties (absorption and emission) and cannot be separated within a cell. In controlled solution studies, this problem of spectral overlap is not a problem, but cellular studies become formidable. First, this problem is rationalized in that the bulk NADH is thought to be ten times larger than NADPH, so emission at 430 nm will mostly be NADH.[11] Second, if cells are manipulated by doses of drugs that only affect NADH, then any change in fluorescence should solely be due to the bulk change of the free and enzyme-bound NADH, not NADPH. These metabolic drugs can be specific to NADH because NADH and NADPH are involved in very different cellular reactions.[15] NADPH is mostly involved in the biosynthesis of fatty acids and steroids, while NADH is involved in ATP production.[15] Therefore, NADH and NADPH in cellular studies will just be referred to as NADH.

1.4 Hypothesis

1.4.1 Solution Studies

We hypothesize that the dissociation constant of NADH-LDH will decrease in heterogeneous crowded environment to reduce the excluded volume effects. For homogenous crowding, however there isn't a drive to reduce steric interactions, we hypothesize that homogenous crowding will stabilize product formation and therefore decrease the dissociation constant. Lastly, we hypothesize that equilibrium constants are also dependent on the concentration, shape, and size of macromolecules.

1.4.2 Cellular Studies

In cellular studies, we hypothesize that NADH also exists as a dynamic equilibrium of free and enzyme-bound, and this equilibrium can quantitatively be probed using non-invasive fluorescent techniques. We believe this natural equilibrium is sensitive to drugs that manipulate metabolism and this manipulation (or shift in free/enzyme-bound NADH) can be observed through our non-invasive techniques.

1.5 Significance of Research

The projected results of this paper will enhance our understanding of how macromolecular crowding (heterogeneous environment with excluded volumes) might affect the reaction kinetics of important classes of biochemical reactions involving NADH. Our results will help distinguish between confinement of the reactants in cages formed by the crowding agents and the homogeneous viscosity. Ultimately, the outcome

of this project would represent an important step towards noninvasive diagnostics at the single cell level using natural biomarkers towards understanding mitochondrial dysfunction in human disease. Our spectroscopy techniques are significant in that we can do quantitative biochemistry, non-invasively, to complement traditional biochemical techniques.

1.6 Thesis Outline

The intrinsic fluorescence of NADH is sensitive to conformational changes (e.g., binding to a protein) and environmental changes (e.g., viscosity, oxygen, pH, macromolecular crowding).[10] In addition, recent reports suggest that free and enzyme-bound NADH exist under dynamic equilibrium in living cells.[10] As a result, a combination of time-resolved fluorescence and associated anisotropy measurements will be used in this thesis as the tools of choice for quantitative and noninvasive approaches for elucidating the NADH-enzyme binding kinetics both in solution and in cells. This project is aimed at elucidating the interplay between confinement and viscosity effects on kinetics involving NADH and lactate dehydrogenase (LDH) as a model system. The results of solution studies will guide our research to further understand the NADH equilibrium in living systems.

Chapter 2: Materials and Cell Culture

2.1 Sample Preparation of Solution Studies

2.1.1 Lactate Dehydrogenase

L-lactate dehydrogenase (type III) from bovine heart was purchased from Sigma-Aldrich. LDH was suspended in ammonium sulfate (2.1 M, pH 6) and stored at 4°C. For each experiment, stock LDH was freshly dialyzed against *Tris* Buffer (100 mM, pH 8.5) using Slide-A-Lyzer MINI Dialysis Device with a molecular cut off weight of 3.5K purchased from Thermo Scientific. Dialysis was done on a Gyrotory shaker-model G2 (4°C, 100 RPM) for 2 hours. The dialyzed buffer was replaced with fresh buffer and then left to dialyze for 12 more hours. Dialyzed LDH was concentrated using an Amicon Ultra-4 centrifuge filter with a molecular cut off weight of 10 k to obtain the desired concentration. Concentrations of LDH were determined using a UV-vis absorbance spectrophotometer (DU800, Beckman coulter). The extinction coefficient for LDH at 280 nm is 16.2 X 10^4 M^{-1} cm^{-1}.[9]

2.1.2 Nicotinamide adenine dinucleotide (NADH)

NADH was purchased from Sigma-Aldrich and used without further purification. NADH was stored in Tris buffer (100 mM, pH 8.5) at 4°C. Concentrations of NADH were determined by using a UV-vis absorbance spectrophotometer (DU800, Beckman coulter). The extinction coefficient for NADH at 340 nm is 6220 M^{-1} cm^{-1}.[9]

2.1.3 Crowding Agents

All crowding agents used (Ficoll−70, Ficoll−400, glycerol, dextran−6, dextran−70, and dextran−150), were prepared the day before experimentation and made in *Tris* buffer (100 mM, pH 8.5) and stored at 4°C to match LDH and NADH's recommended buffer system. According to venders, all polymers purchased have a low polydispersity that are close to 1 (M_w/M_n). Polydispersity is a calculation of how close the molecular weight is to the advertised molecular weight. Ficoll−70 (70,000 kDa), a synthetic polymer of sucrose, was purchased from Santa Cruz Biotechnology, prepared as a 550 g/L stock, and then diluted to desired concentration. Ficoll−400 (400,000 kDa) was purchased from Sigma-Aldrich and prepared in a 400 g/L stock solution. Glycerol (Fluka) was prepared as a 900 g/L stock prior to dilution. Dextran−70 (70,000 kDa), a complex of branched glucan, from Leuconostoc spp, was purchased from Sigma-Aldrich and prepared as a 450 g/L stock. Dextran−6 (6,000 kda) from Leuconostoc spp was purchased from Sigma-Aldrich and was prepared as a 500 g/L stock. Dextran-150 (150,000 kDa) from Leuconostoc Menesteroides, was purchased from Sigma-Aldrich and prepared as a 400 g/L stock solution. Crowding agents were prepared in varying stock concentrations because each has a different solubility.

2.1.4 7-hydroxycoumarin-3-carboxylic acid

7- hydroxycoumarin-3-carboxylic acid (here thereafter, coumarin) was used as a control fluorophore to calculate the geometrical factor (G-factor) of our experimental setup to account for potential polarization-biased detection of NADH emission. Coumarin was

prepared in Tris buffer (100 mM, pH 8.5) as a 50 μM stock solution and then diluted to 10 μM for experiments.

2.2 Cellular Studies

2.2.1 Aseptic Mammalian Cell Culture Protocol

Mouse embryonic fibroblast cell line (C3H10T1/2) was purchased from American Type Culture Collection (ATCC). Fibroblast cells were grown in Dulbecco's Modification of Eagle's Medium (DMEM) with 4.5 g/L glucose, L-glutamine, sodium pyruvate, and Phenol red (10-013-CV). DMEM was supplemented with 10% Fetal Bovine Serum (FBS) for complete growth medium. Cells were grown in T-25 Falcon flasks (Becton Dickinson) with filter caps to prevent microorganism contamination and allow gas exchange. Incubation was done in 37°C and 5% CO_2 in Forma Scientific CO_2 water jacketed incubator. In order to passage cells once confluent (70-90%), medium was removed from the flasks, and 2 mL of Trypsin-EDTA solution was added for 8-10 minutes and incubated at 37°C and 5% CO_2. Trypsinized cells were checked under inverted Olympus microscope after incubation to verify all cells are detached to prevent selection of cells that detached more readily from flask. Cells were not imaged or grown past passage number 20. Cells were frozen in DMEM media with 5% DMSO under liquid nitrogen for long term storage. Prior to imaging cells, cells were transferred to MatTek corporation glass bottom petri-dishes (35mm petri dish, 14mm microwell, number 1.5 coverglass) the day before experimentation. Cells in MatTeck glass bottom petri-dishes received complete medium (DMEM and 10% FBS) without Phenol Red in

order to avoid background fluorescence while imaging. Cells were imaged at room temperature (25°C) and low humidity (5%) for less than 45 min to prevent cellular stress due to pH instability of carbonate buffer in DMEM.

2.2.2 Rotenone for metabolic manipulation

Rotenone is an inhibitor of complex I in the mitochondrial electron transport, halting the oxidation of NADH.[20-22] Analytical standards (≥95%) of this complex I inhibitor were purchased from Sigma-Aldrich (R8875) and used without further purification as recommended by the manufacturer after being diluted in DMSO. Stock solutions (10 μM) were stored in a dark environment at 4°C prior to use. For acute complex I inhibition of C3H10T1/2, cells were incubated with either 1 μM or 10 μM of Rotenone for 15 minutes and washed 3 times with phenol free medium before imaging.

2.2.3 MitoTracker Green FM

MitoTracker Green FM is a green fluorescent mitochondrial stain allowing clear visualization of cell's mitochondrial morphology and distribution. MitoTracker Green FM is beneficial because it is only fluorescent when it accumulates in the lipid membrane of the mitochondria, so excessive washing steps can be omitted. In addition, MitoTracker green FM is far more photostable compared to the traditional mitochondrial stain, rhodamine 123, and should be better resolved. [23] MitoTracker Green FM was purchased from ThermoFisher and was stored at -18 °C in a desiccator and protected from light before use. The excitation and emission of MitoTracker Green is suitable for our laser

system at 490 and 516, respectively, and does not overlap with the emission of NADH (430 nm). MitoTracker Green FM was stored as a 1 mM stock solution in DMSO at 4°C and diluted to 1 µm working solution when staining cells. The diluted MitoTracker was incubated in serum free media due to potential oxidases. After incubation of 15 minutes, MitoTracker filled media is replaced and washed 3 times with phenol free media for imaging.

2.2.4 Rhodamine 123

Rhodamine 123, like MitoTracker Green FM, is a fluorescent dye that is sequestered by active mitochondria.[23] Rhodamine 123 is the most common mitochondrial stain and will be used as a comparative method to MitoTracker for observing the cell morphology and health of the mitochondria. Rhodamine 123 has an excitation and emission of 507 and 529 nm, respectively, so the same excitation and emission filters as MitoTracker can be used here. Rhodamine 123 was purchased from ThermoFisher Scientific and stored at -18 °C in a desiccator and protected from light before use. 5mM stock solutions were prepared in DMSO and stored at 4°C. A working concentration of 1 µM of Rhodamine 123 was incubated in phenol free DMEM for 15 minutes. After incubation, cells were washed with phenol free media 3 times to thoroughly remove free Rhodamine 123. Cells were imaged in phenol free media to prevent background fluorescence from phenol red.

Chapter 3: Methods, Instrumentation, and Data Analysis

3.1 Instrumentation

3.1.1 Time-Correlated Single-Photon Counting Technique

Excited-state dynamics of NADH-LDH mixtures in solution and cells were carried out using time-correlated single-photon counting technique (TCSPC) to determine the fluorescent lifetime of NADH in different environments. A Titanium-Sapphire solid state laser system (Mira 900-F, Coherent) was tuned to generate femtosecond near-infrared laser pulses (120 fs, 76 MHz, 730 nm), which was pulse-picked at 4.2 MHz repetition rate. The laser pulses were steered to an inverted microscope (Olympus IX81) to excite a droplet of the sample on a coverslip positioned on the microscope stage after a 1.2NA, 60x objective. The NADH emission was filtered, and detected by a microchannel plate (MCP) photomultiplier tube (R3809U, Hamamatsu), amplified, and routed to a synchronized SPC-830 module (Becker & Hickl) for single-photon counting and TCSPC measurements.[19, 24] TCSPC methods were used for 2P-lifetime, 2P-anisotropy measurements based on polarization analysis, and 2P-FLIM using laser scanning approach to gain spatial information.

3.1.2 Two-Photon Excitation

Two-Photon excitation (2P) is achieved by the simultaneous absorption of two photons that are of lower energy. Traditionally, (1P) excitation is used to excite NADH to a higher energy state; however, high power excitation using 1P (near UV) can lead to photo-damage of cells and increased scattering of light.[25] Two-Photon excitation is less harsh on live cells due to limited out-of-focus photobleaching, negligible scattering, and has the benefit of deeper penetration into tissue.[10] Usually NADH is excited at 430 nm, but in a (2P) excitation, this is shifted up to the near infrared region of 730 nm (Figure 3.1, blue line) [25], while the emission is detected at 450 nm.

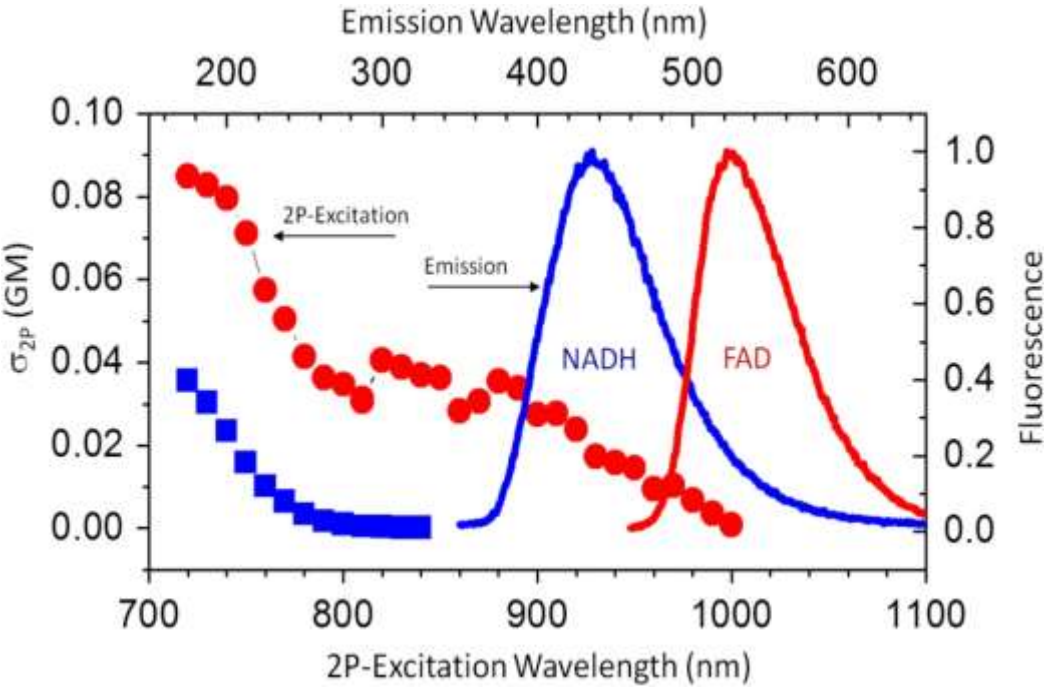

Figure 3.1: 2-Photon excitation and emission of NADH

3.1.3 Two-Photon Fluorescence Lifetime

For fluorescence lifetime measurements, a Glan-Thompson polarizer was used for magic-angle detection, and the acquired fluorescence decays were analyzed using the SPCImage software (Becker & Hickl), where the quality of the fit was judged using both χ^2 and the residual.[9, 19] For magic angle detection, a Glan-Thompson polarizer is set at 54.7° for the laser polarization so that rotational effects on the excited-state dynamics are eliminated.[19] The measured lifetime is the total fluorescence intensity shown in equation 1[19]:

$$\boldsymbol{I}_{54.7^\circ} = \sum_i \boldsymbol{\alpha}_i \boldsymbol{e}^{-\boldsymbol{t}/\boldsymbol{\tau}_i} \quad (1)$$

Because free and enzyme-bound NADH have very distinct fluorescence lifetimes, two species can be resolved in a solution or cell (α_1 and α_2) with two distinct fluorescent lifetimes (τ_1 and τ_2). These measurements are carried out at 4.2 MHz in order to guarantee the same initial conditions at every laser pulse excitation. Generally, the fluorescence intensity, F(t), of a given fluorophore can be described using a multiexponential decay model, depending on the chemical structure and the surrounding environment such that:

$$\boldsymbol{F(t)} = \sum_{\boldsymbol{i=1}}^{\boldsymbol{3}} \boldsymbol{\alpha}_i \boldsymbol{\tau}_i \quad (2)$$

Where, α_i and τ_i are the amplitude fraction and fluorescence lifetime of the i^{th} fluorophore, respectively. The measured fluorescence decay was deconvoluted with a

computer-generated system response function. For a mixture of two species, the fluorescence signal of the i^{th} species will depend on both the population fraction and the fluorescence quantum yield (or lifetime) of that species such that:

$$\boldsymbol{f_1} = \frac{\boldsymbol{\alpha_1 \tau_1}}{\sum_{\boldsymbol{i=1}}^{\boldsymbol{3}} \boldsymbol{\alpha_i \tau_i}} \quad (3)$$

3.1.4 Two-Photon Florescence Anisotropy

For anisotropy measurements, randomly oriented fluorophores in a solution or a cell (Figure 3.2 A) can be photoselectively excited when their dipole are aligned with the excitation laser pulse, λ(E). Following polarized pulsed excitation, these vertically aligned fluorophores will rotate or tumble, causing the fluorescence to be depolarized (Figure 3.2 B).[11, 13, 19, 26] A polarizing beam splitter was used to isolate and resolve the parallel and perpendicular fluorescence polarizations (with respect to the laser polarization), which were detected simultaneously using two Microchannel Plate Detector's (MCPs). Because free and enzyme-bound NADH have very different molecular weights, their respective rotational times are distinct. These very different rotational times can also be used to elucidate the ratio of free and enzyme-bound NADH in a solution or cell.

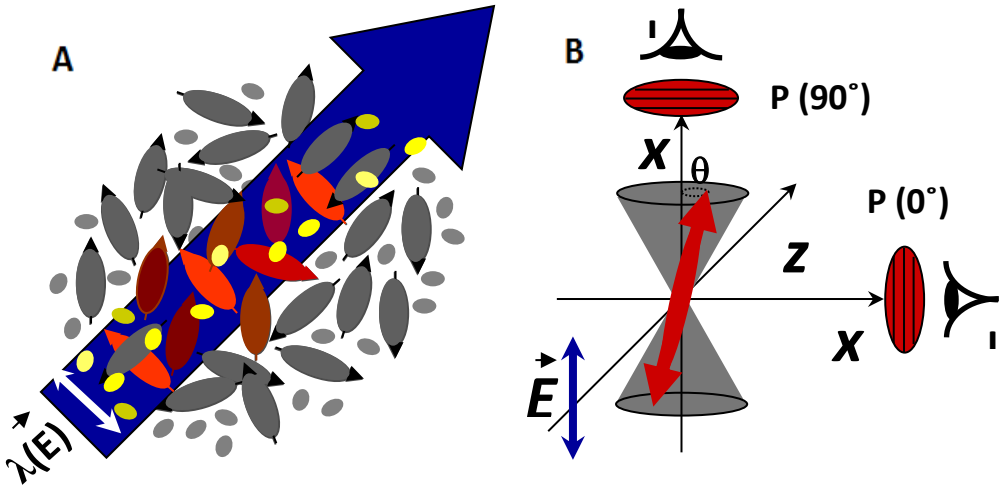

Figure 3.2: (A) A solution of randomly oriented fluorophores being preferentially excited by the excitation source. (B) Vertically aligned fluorophores become depolarized due to tumbling.

For time-resolved anisotropy, the measured parallel and perpendicular fluorescence decays are used to calculate the anisotropy decay such that[19]:

$$r(t) = \frac{I_{\perp}(t) - GI_{\parallel}(t)}{I_{\perp}(t) + 2GI_{\parallel}(t)} = \sum_i \beta_i e^{-t/\varphi_i} \quad (4)$$

Steady-state anisotropy methods will be touched on briefly, and can simply be related to time-resolved anisotropy by equation 5[19]:

$$r_{ss} = \frac{\int I_{\perp}(t) - \int GI_{\parallel}(t)}{\int I_{\perp}(t) + 2\int GI_{\parallel}(t)} \quad (5)$$

The steady-state anisotropy (r_{ss}) is simply the angle between the absorbing and emitting dipole and is analogous to time-resolved anisotropy at time zero (r_o).[19] Steady-state anisotropy are complementary methods to time-resolved and will further reveal how rotational dynamics are affected by crowding.

The geometrical factor (G-factor) was also determined using tail-matching approach.[13] Because the emission passes through both perpendicular and parallel filters, the G-factor is calculated to account for the potential biases between the two filters.[19] Before each experiment, a small molecule, coumarin with a known rotational time, was used as a control to calculate the G-factor where a calculated G-factor of one shows no biases between filters (equation 6).[19]

$$\boldsymbol{G = \frac{I_{\parallel}(t)}{I_{\perp}(t)}} \tag{6}$$

For an ensemble of two molecular species (e.g., free and enzyme-bound NADH), each of which has a distinct fluorescence lifetime (τ_i) and rotational time (φ_i) due to differences in their size, the corresponding time-resolved associated anisotropy curves are described as following.[19]

$$\boldsymbol{r(t) = \frac{\sum_{i=1}^{N_{free}} \alpha_i \exp(-\frac{t}{\tau_i}) \cdot \beta_i \exp\left(-\frac{t}{\varphi_i}\right) + \sum_{j=1}^{M_{bound}} \alpha_j \exp(-\frac{t}{\tau_j}) \cdot \beta_j \exp(-\frac{t}{\varphi_j})}{\sum_{i=1}^{N_{free}} \alpha_i \exp(-\frac{t}{\tau_i}) + \sum_{j=1}^{M_{bound}} \alpha_i \exp(-\frac{t}{\tau_j})}} \tag{7}$$

The corresponding pre-exponential factors, α_i and β_i, represent the relative population of each species in the mixture. It is worth mentioning that the denominator of equation (4) can be measured independently using magic-angle polarization detection as described above (equation 1). Such complementary approach does reduce the number of independent variables during the nonlinear least square fitting of the measured associated anisotropy. Equation (4) can be rewritten in terms of lifetime-dependent amplitude fractions of the free (f_1) and enzyme-bound (f_2) NADH such that:

$$\boldsymbol{r(t) = f_1(\tau)_1 \cdot r_1(\varphi_1) + f_2(\tau)_2 \cdot r_2(\varphi_2)} \quad (8)$$

where the amplitude fractions are defined as:

$$\boldsymbol{f_1 = \frac{\alpha_1 e^{-t/\tau_1}}{\alpha_1 e^{-t/\tau_1} + \alpha_2 e^{-t/\tau_2}}}, \text{ and } \boldsymbol{f_2 = \frac{\alpha_2 e^{-t/\tau_2}}{\alpha_1 e^{-t/\tau_1} + \alpha_2 e^{-t/\tau_2}}} \quad (9)$$

In these equations, it is assumed that the two species in the mixture have independent fluorescence lifetime and size-dependent rotational time. These assumptions are consistent with the notion that the fluorescence lifetime of NADH is sensitive to protein binding.[19] In addition, it is safe to assume that the enzyme-bound NADH would have larger hydrodynamic radius (V) as compared with the free counterpart where the rotational time (φ) is positively correlated such that:[19]

$$\varphi = \frac{\eta V}{K_B T} \quad (10)$$

Equation 10 (a modified version of the Debye-Stokes-Einstein relation) also shows the relationship of the local viscosity (η), temperature (T), and the Boltzmann constant (K_B). The anisotropy decays were analyzed using OriginPro software without deconvolution of the system response function (FWHM~50 ps).

3.1.5 Differential Interference Contrast (DIC) and Confocal Microscopy

Compared to traditional bright field microscopes, DIC imaging techniques can be used to greatly increase the contrast and spatial resolution of images to assess cellular morphology without fluorescent labeling.[27-28] In addition to DIC, confocal imaging was used to further assess cell and mitochondria morphology through fluorescence. The excitation source will excite all fluorophores that are within the illuminated cone. Emitted light will pass through a dichroic mirror that only allows our fluorescence of interest to transmit and all other light to be reflected. The out-of-focus fluorescence will be neglected by a confocal pinhole in front of the detectors. Both confocal, DIC images can be simultaneously collected and compared side-by-side. The confocal microscope used here consists of an inverted microscope (Olympus, IX81) and a laser scanning unit (Olympus, FV300). The excitation lasers consist of an argon ion laser (350, 488, 514 nm) and helium-neon laser (543 and 633 nm) which will allow us to excite different fluorescent markers. The laser lines were focused on the cultured cells that were grown in MaTeck glass bottom petri dishes using a 1.2 NA and 60X water immersion microscope

objective (IX81, Olympus). In these confocal images, the fluorescence signals from cell treated with Rhodamine 123 or MitoTracker Green FM were detected using a 520F Emission filter with a 488 nm excitation line from the argon laser.

3.1.6 Two-Photon Fluorescence Lifetime Imaging Microscopy (FLIM)

2P-FLIM produces images based on fluorescent lifetimes of fluorophores rather than fluorescence intensity, as seen in confocal microscopy.[19] In contrast with fluorescence intensity, fluorescence lifetime is very sensitive to molecular structure (e.g. binding) and environment. In addition, the fluorescence lifetime is independent from the concentration of the fluorophore. In FLIM, we can excite NADH molecules in the cell and quantitatively measure their respective fluorescence lifetimes. Fluorescent lifetimes of NADH are sensitive to both the chemical structure and the surrounding environment. This sensitivity of NADH to its change in molecular structure can reveal the fraction of bound and free NADH. The experimental setup used in our two-photon fluorescence lifetime imaging (2P-FLIM) is described elsewhere.[29] Briefly, for FLIM measurements, two-photon epifluorescence signal was detected at magic-angle (54.7°) using a Glan Thompson polarizer, with respect to the excitation laser polarization, by a microchannel plate photomultiplier tube, or MCP-PMT (R3809U, Hamamatsu, Hamamatsu City, Japan) prior to amplification and detection using a SPC-830 module (Becker & Hickl, Berlin, Germany). Unlike single-point fluorescent-lifetime measurements, 2P-FLIM is based on 2P-laser scanning at 76 MHz in order to gain spatial information concerning the lifetime heterogeneity throughout the cell. For proper control of the fluorescence

polarization state, the DIC polarizer in the inverted microscope was removed during FLIM measurements. The average power of the femtosecond laser pulses at the samples were reduced enough (~5 mW) in order to avoid cellular stress of photodamage. In each fluorescence lifetime image (256 x 256 pixel image with 256 time bins per pixel), the fluorescence decay per pixel, measured at magic-angle, was analyzed using SPCimage 4.8 (Becker & Hickl, Berlin, Germany) for a non-linear least squares fitting. The intrinsic NADH autofluorescence decays in each pixel (x,y) of the acquired FLIM images were described using a biexponential decay model.

3.1.7 Two-Photon Fluorescence Anisotropy for Cellular Studies

In section 2.1.4 (Two-Photon Fluorescence Anisotropy), the free NADH and enzyme bound NADH are expected to have distinct lifetimes and distinct rotational times in solution, and these population fractions can be calculated. This same method can be implemented in cellular studies to study intrinsic NADH. The only difference is that scanning mode is used, rather than single point measurements, over the whole cell to avoid cellular damage.[30]

3.2 Quantitative Methods for Elucidating Enzyme-Bound NADH

Consider the following reaction mechanism for NADH and LDH, where:

$$\boldsymbol{n\,NADH + LDH \leftrightharpoons LDH(NADH)_n} \tag{11}$$

Where the equilibrium constant is defined as:

$$\boldsymbol{K_{eq} = \frac{[LDH(NADH)_n]}{[LDH]\cdot[NADH]^n} = K_d^{-1}} \tag{12}$$

In addition, the fractions of free and LDH-bound NADH can be written as:

$$\boldsymbol{f_1 = \frac{[NADH]}{[NADH]+[LDH(NADH)_n]}}, \text{ and } \quad \boldsymbol{f_2 = \frac{[LDH(NADH)_n]}{[LDH]+[LDH(NADH)_n]}} \tag{13}$$

In our experimental design, we considered the initial LDH concentration to be our independent variable for practical reasons. In this case, we started with the minimum concentration of NADH that would yield acceptable 2P-fluorescence signal level under our experimental conditions (200 μM). The relative LDH concentration in the reaction mixture was then varied prior to measurements. Using the initial conditions and mass conservation, equation (12) can be rewritten as a function of the initial (rather than the equilibrium) concentration of LDH where:

$$f_2 = \frac{[LDH]}{K_d + [LDH]} \quad (14)$$

Our time-resolved anisotropy were fit satisfactorily using equation (7). The corresponding enzyme-bound fraction of NADH, equation (13), was then plotted against [LDH] and fit using equation (14) for K_d quantification as a function on the environment. A similar approach was applied using time-resolved fluorescence measurements as a means to independently determine the corresponding K_d of this NADH-LDH reaction. Here, we assigned fast fluorescence decays component to free NADH while the slow decay component to the enzyme-bound NADH. To estimate the bound fraction of NADH using fluorescence lifetime measurements, we used the following equation:

$$f_B = \frac{<\tau_{fl}>}{\tau_1} = \frac{\gamma[LDH]}{K_d + [LDH]} + \frac{K_d}{K_d + [LDH]} \quad (15)$$

Where $<\tau_{fl}>$ is the average lifetime, τ is the fluorescence lifetime of the free NADH, and γ is the fluorescence enhancement factor of NADH upon enzyme binding.

Chapter 4: Homogenous Crowding Effects on NADH-LDH Binding

4.1 Rationale

Cellular environments are heterogeneous with compartments that have varying viscosity as well as crowding due to the presence of macromolecules. In this chapter, we investigate the effects of homogenous, bulk viscosity on NADH-LDH binding using glycerol-enriched buffer. Our hypothesis is that homogenous crowding will stabilize product formation and therefore decrease the dissociation constant. To test this hypothesis, we carried out both time-resolved fluorescence lifetime and associated anisotropy of NADH-LDH in buffer and as a function of glycerol concentration.

4.2 Enhancement of Fluorescence lifetime Upon Enzymatic Binding

Figure 4.1 shows the normalized fluorescent lifetime plotted as a function of the normalized [LDH] concentration. The average fluorescent lifetime $<\tau>$, of free NADH, was used to normalize every ratio of [NADH]:[LDH] mixture (1:0, 32:1, 16:1, 8:1, 5:1, 4:1, 2:1, and 1:1). As the concentration of LDH increases, a higher fraction of NADH becomes bound, where the last data point shown is fully bound NADH. Equation (15) was used to fit experimental data to estimate the enhancement factor (γ). The enhancement factor quantitatively shows the fluorescent lifetime of free NADH increased by (3.5−4.0 ns), when fully bound to LDH. Our results reveal that fully bound NADH has an average fluorescence lifetime that is 3.25-times larger than that of the free NADH (0.45 ns) in a *Tris* buffer at room temperature. This indicates that the fluorescent lifetime

of NADH is significantly dependent on enzyme binding. As a result, we will exploit these findings to quantify the population fractions of free and enzyme-bound NADH towards noninvasive, quantitative biochemical kinetics in both biomimetic and cellular environments.

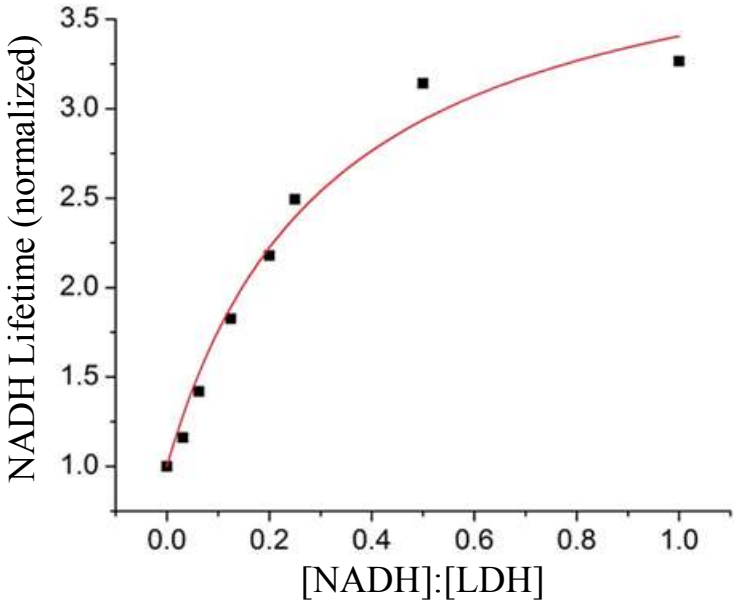

Figure 4.1: Two-photon fluorescence lifetime enhancement of NADH as a function of LDH binding in *Tris* buffer. The fluorescence of NADH decays as a biexponential and the corresponding average fluorescence lifetime of NADH, normalized to that of free NADH in a buffer, is shown as a function of LDH binding. The fitting model used here provides the dissociation constant (K_d) and the lifetime enhancement factor of NADH upon LDH binding. In these measurements, the NADH concentration was 200 μM while LDH concentration ratio was varied (0-1:1).

4.2 Homogenous Crowding Effects on NADH-LDH Binding Kinetics

4.2.1 Time-Resolved Two-Photon Fluorescence Lifetime Approach

The excited state dynamics of NADH is sensitive to enzyme binding (shown in Figure 4.1), which can be quantified using fluorescence lifetime measurements. We used two-photon (2P) fluorescence lifetime, a noninvasive and quantitative methods, to study how homogenous crowding affects the binding kinetics of NADH-LDH complex under controlled conditions. We investigated the binding kinetics as a function of the concentration of [NADH]:[LDH] mixtures in glycerol, to simulate a homogenous environment. The viscosity of cytoplasm in mammalian cells are estimated to be in the range of 2-4 cP, which is in the range of 200−400 g/L glycerol.[31] Using SPCImage software, the raw lifetime decays were fit to either a biexponential or triexponential based on both χ^2 and the residual. The Summaries of fitting parameters for homogenous environments (*Tris* buffer, glycerol 200 g/L and glycerol 400 g/L) are found in Table 4.1.

Table 4.1: A summary of the fitting parameters of time-resolved fluorescence of NADH as a function of both LDH concentration and the environment (*Tris* buffer, glycerol 200g/L, glycerol 400g/L).

Environment: [NADH]:[LDH]	α_1	τ_1 (ns)	α_2	τ_2 (ns)	α_3	τ_3 (ns)	f_b (%)	K_d (μM)
Tris Buffer:								0.1000
1:1	0.72	1.019	0.280	2.004	--	--	1	±
2:1	0.67	0.933	0.329	1.887	--	--	1	0.02257
4:1	0.50	0.496	0.425	1.304	0.079	2.286	0.75	
5:1	0.58	0.445	0.361	1.252	0.061	2.331	0.70	
8:1	0.66	0.396	0.280	1.147	0.063	2.167	0.64	
16:1	0.72	0.354	0.230	0.879	0.051	2.027	0.18	
32:1	0.58	0.297	0.380	0.590	0.036	1.790	0.14	
1:0	0.77	0.334	0.234	0.620	--	--	0	
Glycerol Enriched Buffer (200 g/L)								0.087 ± 0.01766
1:1	0.57	0.993	0.36	1.937	0.075	2.549	1	
2:1	0.54	0.911	0.38	1.898	0.08	2.348	1	
4:1	0.49	0.502	0.42	1.436	0.09	2.598	0.77	
5:1	0.55	0.451	0.36	1.350	0.095	2.414	0.74	
8:1	0.66	0.412	0.27	1.298	0.067	2.479	0.66	
16:1	0.72	0.367	0.21	0.970	0.069	2.164	0.24	
32:1	0.73	0.349	0.22	0.771	0.047	2.038	0.18	
1:0	0.79	0.343	0.21	0.705	– –	– –	0	
Glycerol Enriched Buffer (400 g/L)								0.058 ± 0.00909
1:1	0.51	1.004	0.40	2.053	0.093	2.805	1	
2:1	0.53	1.02	0.38	2.166	0.091	2.806	1	
4:1	0.47	0.669	0.43	1.805	0.1	3.010	0.78	
5:1	0.45	0.507	0.45	1.557	0.097	3.085	0.81	
8:1	0.61	0.469	0.31	1.541	0.073	2.899	0.71	
16:1	0.75	0.426	0.19	1.232	0.065	2.584	0.55	
32:1	0.73	0.389	0.21	0.863	0.053	2.370	0.21	
1:0	0.82	0.388	0.19	0.770	– –	– –	0	

It is important to note that although free NADH and enzyme-bound NADH have very distinct fluorescence lifetimes and rotational times, free NADH can also have two distinct lifetimes because NADH is flexible in structure (folded and stretched). As shown in Table 4.1, free NADH has two components (α_1 and α_2) with their respective lifetime's τ_1 and τ_2 were assigned as only free NADH (folded and stretched). Because both components are unbound, the calculated fraction of enzyme-bound NADH is zero (using equation 13). When mixtures of NADH and LDH were measured, the assigned fractional population (α) and the corresponding fluorescence lifetime (τ) of free and bound NADH are a very different, and each case had to be discerned independently. For example, the fluorescence of [NADH]:[LDH] = 16:1, exhibits three decay components with the bound fraction (α_3). In 16:1 we see two shorter lifetimes (τ_1 and τ_2), where these were assigned to free NADH. At the third component (τ_3), this lifetime is much larger and was assigned to enzyme-bound component. With the correct assignments of free and bound NADH, the fraction bound of NADH can be calculated (equation 13). We assigned fluorescence decay components with a fluorescence lifetime > 1.0 ns as bound NADH. This assumption is reasonable because much longer lifetimes (>1 ns) are never seen in pure NADH samples. In addition, our result of lifetime enhancement shown in Figure 4.1 supports our assignment. The calculated bound fraction of NADH was plotted as a function of [LDH] concentration. Results for a buffered solution are shown in Figure 4.2, where the fraction of LDH-bound NADH was zero and 1.0 at [LDH]:[NADH] = 0 and 1.0, respectively. Using equation (15), we estimated a dissociation constant (K_d) of 0.1 ± 0.023 in *Tris* buffer at room temperature (Shown in Table 4.1).

Each Glycerol 200 g/L and Glycerol 400 g/L were plotted and fit in the same fashion, where the dissociation constants are reported in Table 4.1. Our results show that the observed dissociation constant of $LDH(NADH)_n$ complex decreases with increased glycerol concentration (200 and 400 g/L) as compared with that in *Tris* buffer. This suggests that glycerol stabilizes enzymatic binding upon mixing.

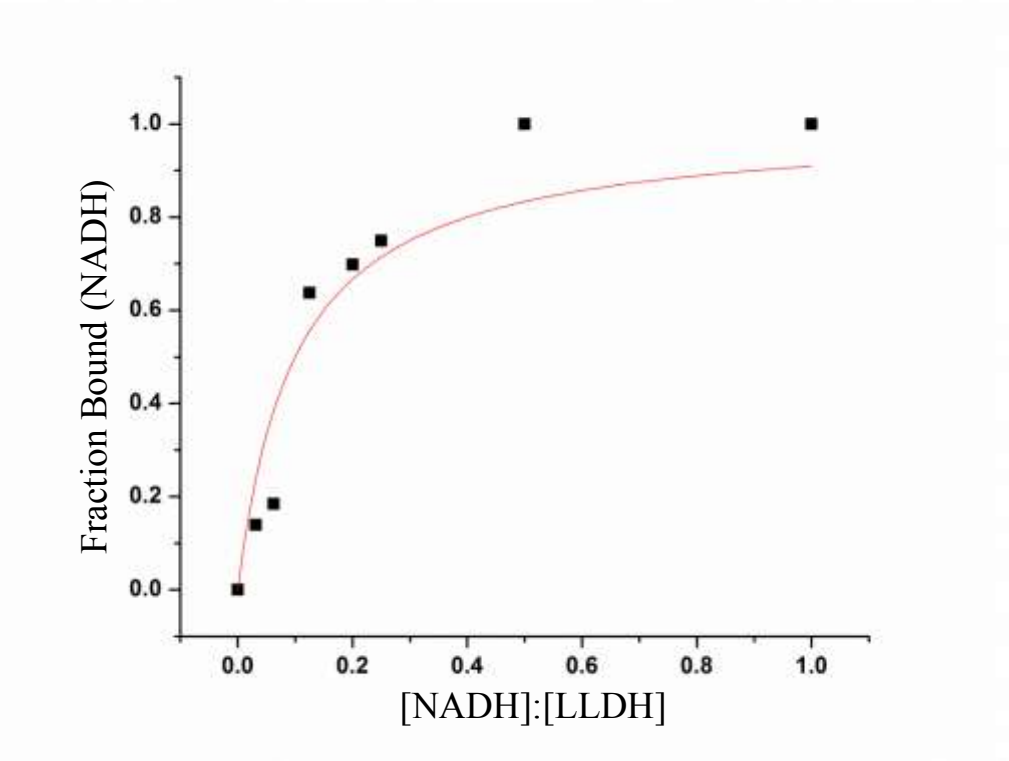

Figure 4.2: The NADH-bound fraction in NADH-LDH mixture was calculated using two-photon time-resolved fluorescence as a function of LDH titration in a buffer (*Tris*, pH 8.5, room temperature). The slow fluorescence lifetime in the multi-exponential decays was assigned as NADH-LDH bound species. The corresponding NADH-LDH bound fraction was then calculated as a function of LDH concentration. The fitting curve yields an estimated K_d of 0.1 ± 0.023 μM in pure *Tris* buffer at room temperature.

4.2.2 Time-Resolved (2P)-Fluorescence Anisotropy Approach

There are a few challenges associated with fluorescence lifetime measurements as a means for investigating the crowding effects on NADH-LDH reaction kinetics. For example, the NADH fluorescence in pure buffer decays as double exponential, while triple exponential decays were observed in the presence of LDH. The excited state lifetime is also known to be sensitive to many environmental factors such as the viscosity (and pH) surrounding the structurally flexible fluorophores such as NADH.[10] Finally, the refractive index of crowded environments is expected to influence the radiative rate constant and therefore the fluorescence decay rate of NADH according to Strickler-Berg equation.[18] To overcome these challenges, we carried out time-resolved (2P)-anisotropy of NADH-LDH reaction as a function of the concentration of glycerol as a comparative method to (2P)-Lifetime. Time-resolved anisotropy yields the rotational time, which is sensitive to the size of fluorophore such as free and bound NADH. Considering the size difference between free and enzyme-bound NADH, time-resolved anisotropy seems to be the method of choice for a quantitative, noninvasive approach for reversible chemical reaction. On the nanosecond timescale, reactants (e.g., NADH) and products (e.g., LDH-NADH complex) are almost frozen in space, which allow us to ignore translational diffusion. The inherent challenges in time-resolved anisotropy of NADH-LDH reaction are two-fold: First, both the fluorescence lifetime and hydrodynamic radius of NADH vary upon binding with LDH, which yields an associated anisotropy profile.[10] As shown in equation 7 for associated anisotropy, there are a total of eight fitting parameters for an associated anisotropy decay. Luckily, four of these fitting parameters (α_1, α_2, τ_1, and τ_2)

can be measured independently using the fluorescence lifetime measured directly at magic angle detection. Second, the overall rotation of a large complex such as $LDH(NADH)_n$ is too slow as compared with the fluorescence lifetime of NADH, which is our window of observation for rotational dynamics. Even though we increased our signal-to-noise (S/N) ratio using reasonably long data acquisition time, the uncertainty of the overall rotational time (and therefore the estimated hydrodynamic volume) increases with large fluorophores. Shown in Figure 4.3, the anisotropy decay curves for both free NADH and Fluorescein are shown. Both NADH and Fluorescein are fluorescent molecules, but only NADH is flexible and therefore decays as a bi-exponential. This concept that free NADH has two distinct rotational times and fluorescence lifetimes will be important for data analysis.

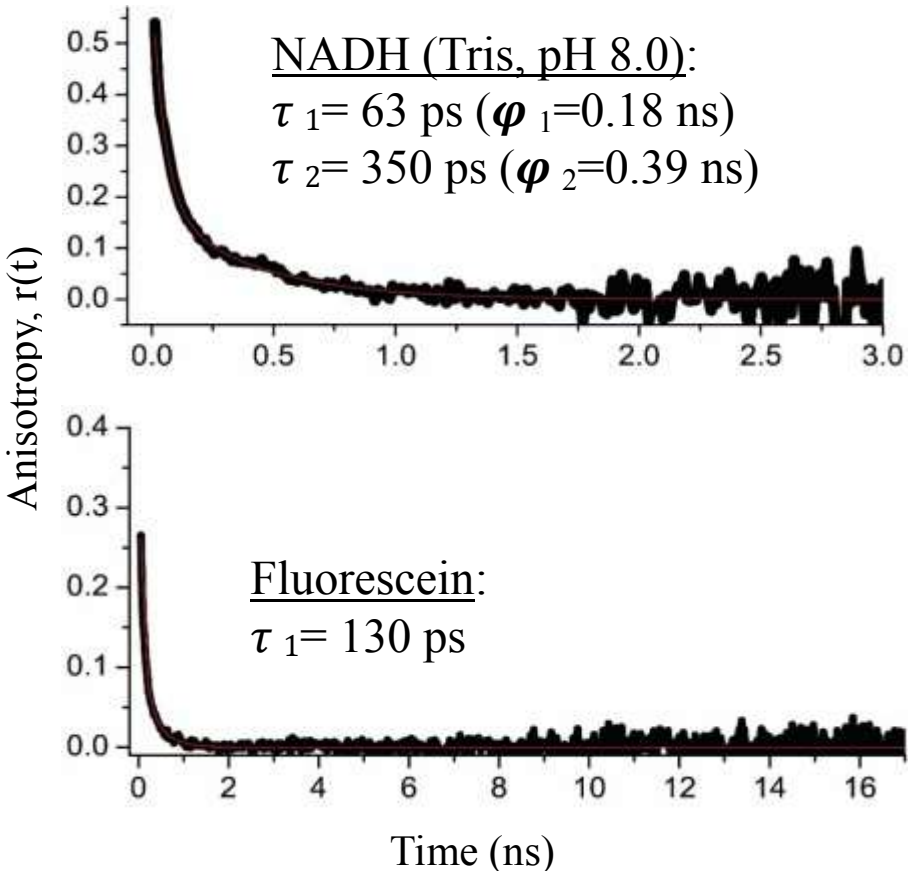

Figure 4.3: Two-photon florescence anisotropy decay of NADH and Fluorescein. NADH decays as a biexponential (two distinct fluorescent lifetimes and two distinct rotational times) because NADH is flexible. Fluorescein fits to a single exponential because it is more rigid and only shows one distinct lifetime and one distinct rotational time.

The anisotropy of free NADH (0.0 μM LDH) decays predominantly as a biexponential, while fully bound (200 μM LDH) NADH decays predominantly as a single exponential with estimated rotational times of 0.1/0.4 ns and 51 ns, respectively, in pure *Tris* buffer at room temperature. These overall rotational times are consistent with the corresponding hydrodynamic volumes (equation 10). As the relative concentration ratio of [NADH]:[LDH] varied, associated anisotropy profiles were observed over the range of 32:1 to 2:1 due to changes in the fluorescence lifetime of both free and enzyme-bound species. The free NADH in the mixture rotates on 0.1 - 0.2 ns time scale as compared

with >56 ns for the bound species. The plotted associated anisotropy curves are fit to equation 7, and a representative graph of NADH-LDH mixtures in *Tris* buffer at room temperature is shown in Figure 4.4.

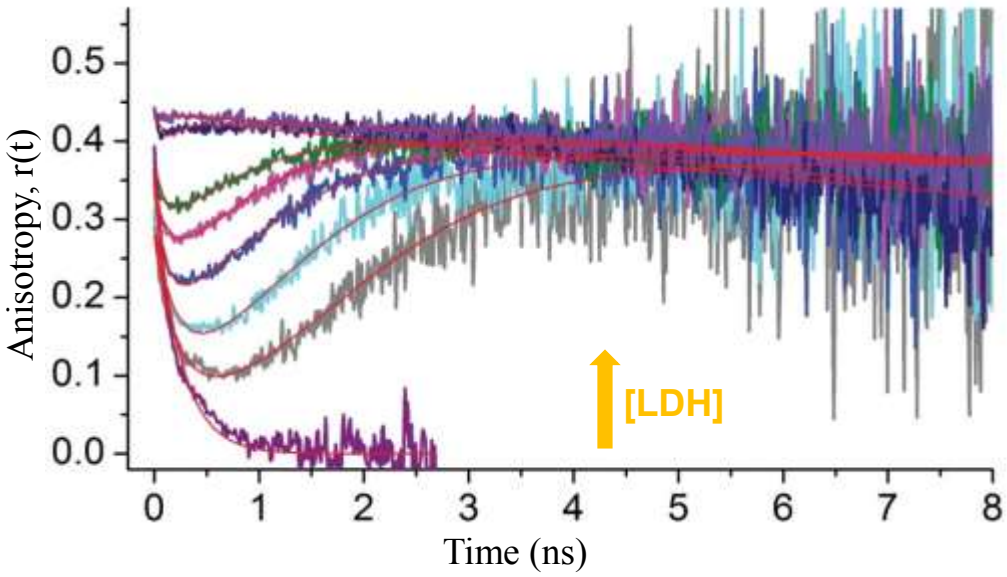

Figure 4.4: Two-photon fluorescence anisotropy curves of NADH are sensitive to LDH titration. A mixture of NADH and LDH exhibit an associated anisotropy that suggest two species of distinct fluorescence lifetime and hydrodynamic size at equilibrium. The [NADH]:[LDH] ratios used in these experiments were 1:0, 32:1, 16:1, 8:1, 5:1, 4:1, 2:1 and 1:1. The anisotropy of free NADH (200 μM) in a Tri buffer (pH 8.5) is also shown and decays as a biexponential, which is assigned to folded and stretched NADH structure. The anisotropy of a fully bound NADH (at 1:1 concentration ratio) decays as a single exponential with a rotational time of 51.5 ns (see Table 4.2 below).

Figure 4.4 shows a gradient of [NADH]:[LDH] concentrations from 1:0, 32:1, 16:1, 8:1, 5:1, 4:1, 2:1, to 1:1. A solution mixture of 1:0 [NADH]:[LDH] is observed where there is only one species (NADH) and two rotational time, because of the inherent flexibility of NADH. The two rotational times of free NADH are not disparate enough to show associated anisotropy curves, and decay as a biexponential. As the concentration of LDH

increase, a larger fraction of NADH becomes bound to LDH and associated anisotropy curves become apparent. In associated anisotropy curves, there are large difference in rotational times (free NADH and enzyme-bound NADH), and the fast and long rotational times can qualitatively be observed. When there is a mixture of [NADH]:[LDH], the fast rotational time of free NADH can be observed by the quick anisotropy decay, and at later times, the slow rotational time of bound NADH becomes apparent. At 32:1 [NADH]:[LDH], there is a large component of free NADH and a small component of bound NADH. At the ratio of 1:1, all NADH present in the solution becomes fully bound, so there is no fast rotational decay of free NADH observed and an associated anisotropy curve is no longer detected. These distinct rotational times are associated with a fluorescence lifetime (τ) and a fraction of that species (α). A Summary of all NADH-LDH associated anisotropy fitting parameters, in homogenous environments, are shown in Table 4.2.

Table 4.2: A summary of the fitting parameters of time-resolved associated anisotropy of NADH as a function of both LDH concentration and the environment (Tris buffer, glycerol 200 g/L and glycerol 400 g/L).

Environment: [NADH]:[LDH]	β_1	φ_1 (ns)	β_2	φ_2 (ns)	r_0	f_b (%)	K_d (μM)
Tris Buffer:							0.0722
1:1	−−	−−	0.43	51.50	0.44	1	±
2:1	0.51	0.10	0.43	30	0.44	0.98	0.00853
4:1	0.25	0.10	0.43	57.30	0.37	0.82	
5:1	0.24	0.20	0.41	86.90	0.35	0.70	
8:1	0.29	0.11	0.46	24.90	0.36	0.57	
16:1	0.26	0.22	0.39	203	0.31	0.47	
32:1	0.26	0.23	0.37	6.23E26	0.31	0.28	
1:0	0.23	0.08	0.18	0.40	0.39	0	
Glycerol-Enriched: (200g/L)							0.0619 ±
1:1	−−	−−	0.46	86.36	0.46	1	0.00695
2:1	−−	−−	0.45	94.28	0.43	1	
4:1	0.18	0.15	0.44	85.44	0.38	0.84	
5:1	0.25	0.15	0.44	50.70	0.38	0.78	
8:1	0.29	0.23	0.42	87.24	0.36	0.64	
16:1	0.28	0.24	0.46	27.77	0.35	0.46	
32:1	0.28	0.35	0.36	183.82	0.33	0.31	
1:0	0.18	0.13	0.16	0.97	0.34	0	
Glycerol-Enriched: (400g/L)							0.0493 ±
1:1	−−	−−	0.45	167.10	0.44	1	0.00704
2:1	−−	−−	0.45	165.26	0.45	1	
4:1	0.27	0.06	0.47	66	0.41	0.89	
5:1	0.40	0.13	0.44	216	0.39	0.88	
8:1	0.36	0.22	0.45	110	0.36	0.73	
16:1	0.33	0.30	0.48	40	0.33	0.51	
32:1	0.32	0.38	0.59	13.60	0.31	0.30	
1:0	0.08	0.06	0.33	0.72	0.32	0	

Each environment shown (buffer, glycerol 200 g/L, glycerol 400 g/L), the raw (2P)-anisotropy data, was fit to the associated anisotropy equation (7) in order to calculate the bound fraction of NADH. The estimated dissociation constant from these measurements in buffer is 0.072 ± 0.009 μM based on the fitting of equation (14). The estimated dissociation constant in glycerol enriched buffer (200 g/L) decreases to 0.061 ± 0.007 μM and further decreases to 0.049 ± 0.007 μM in glycerol (400 g/L). This same trend was seen in (2P)-fluorescent lifetime measurements and is in agreement. Figure 4.5 shows a summary to compare (2P)-lifetime and (2P)-anisotropy dissociation constants in homogenous environments.

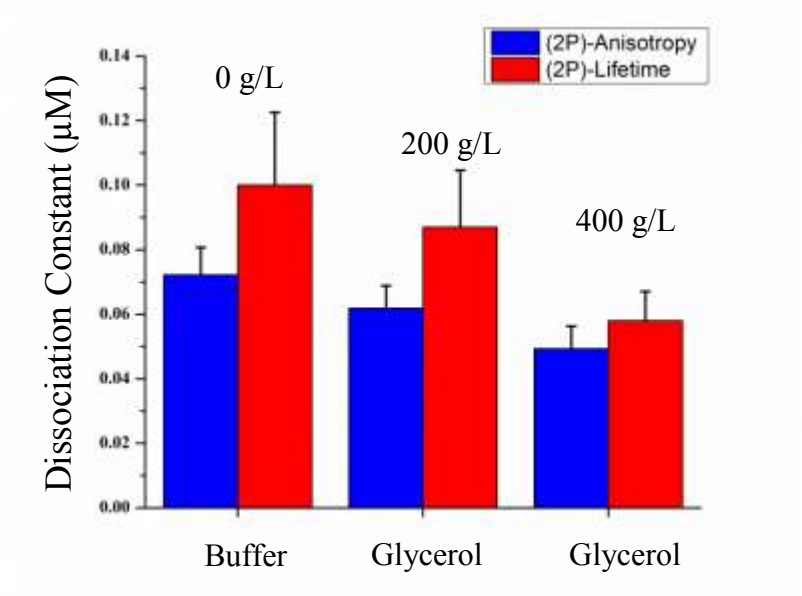

Figure 4.5: The dissociation constant (K_d) of NADH-LDH interactions is sensitive to homogeneous environments (glycerol) Using both the time-resolved fluorescence and associated anisotropy curves, the corresponding dissociation constant of NADH-LDH reaction was calculated. Error bars indicate the standard error of our fit

The results of associated anisotropy and lifetime methods, in a homogenous environment, reveal that an increased viscosity favors product formation, at equilibrium. In these homogenous samples, there is no excluded volume, so product formation is not hindered. When NADH does bind to LDH, the increased viscosity has the potential to stabilize the product (NADH-LDH), making dissociation unfavorable. In addition, here, the dissociation constant is consistently larger for lifetime compared to anisotropy. Based on the uncertainty of the rotational time for large molecules (NADH-LDH), this has the potential to skew the rest of the 7 parameters in the associated anisotropy fit.

Chapter 5: Heterogeneous Crowding effects on Kinetics

5.1 Excluded Volume and Size Dependency of Heterogeneous Crowding

To distinguish between homogenous and heterogeneous effects on kinetics, similar measurements (2P-lifetime and 2P-anisotropy) were carried out using NADH-LDH mixtures in Ficoll−70 enriched buffer (200 g/L and 400 g/L). Ficoll−70 is described as a water soluble, hard sphere polymer that "excludes volume" or occupies space that becomes inaccessible to reactants in the solution.[1, 7, 32-34] Excluded volume studies are important because cellular macromolecules are estimated to occupy up to 30−40% of available space within a cell (100–400 g/L), while well mixed solution (*in vitro*), have a concentration of less than 10 mg/mL.[34-36] It is thought that this excluded volume will have considerable effects on reaction kinetics.[7] Because the inside of a cell has many different sizes of macromolecules, Ficoll−400 (200 g/L) enriched-buffer was also carried out in solution and the dissociation constant was calculated. Ficoll is an inert polymer used here to allow us to separate the effects of excluded volume and electrostatic interactions,[32] which may be present with other crowding that may carry a surface charge. Ficoll−400 at 400 g/L was not measured because of solubility constraints. Our (2P)-lifetime results reveal, in a Ficoll−70 crowded (200 g/L) environment, the dissociation constant of $LDH(NADH)_n$ complex is larger than that of pure buffer at room temperature. This means that the corresponding association constant in the presence of 200 g/L Ficoll−70 is smaller than that of homogeneous, pure buffer. As we increased the Ficoll−70 concentration to 400 g/L, the dissociation (association) constant increased (decreased)

slightly (0.1246 ± 0.03 μM) as compared with 200 g/L. For (2P)-anisotropy comparative measurements, the same trend of the calculated K_d was observed for Ficoll−70 (200 g/L and 400 g/L). Based on the associated anisotropy fitting parameters and plots of fraction bound (NADH) as a concentration of [LDH], these time-resolved anisotropy measurements were estimated to be K_d = 0.12 ± 0.02 μM (200 g/L Ficoll-70) and K_d = 0.15 ± 0.03 μM (Ficoll−70 400 g/L). Interestingly, the dissociation constant in the presence of a much larger crowding agent, Ficoll−400 (200 g/L), was greatly reduced. The estimated dissociation constant for Ficoll−400 (200 g/L) for lifetime and anisotropy were 0.07 ± 0.02 μM and 0.05 ± 0.004 μM, respectively. Figure 5.1 shows a summary to compare 2P-lifetime and 2P-anisotropy dissociation constants in heterogeneous environments.

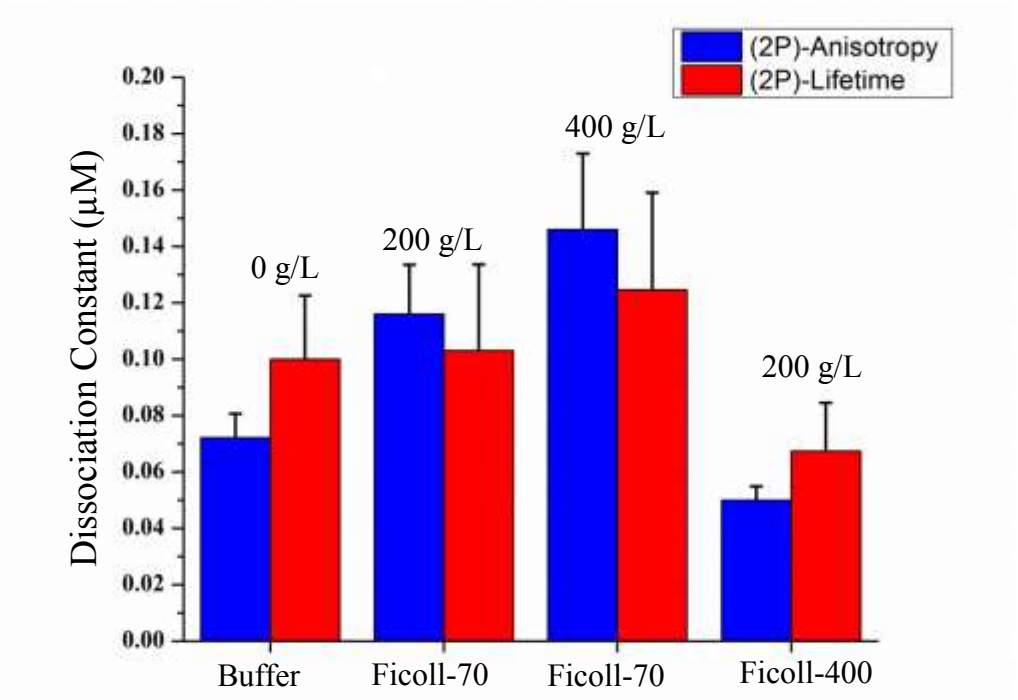

Figure 5.1: The dissociation constant (K_d) of NADH-LDH interactions are sensitive to heterogeneous environments (Ficoll-70 and Ficoll-400) Using both the time-resolved fluorescence and associated anisotropy curves, the corresponding dissociation constant of NADH-LDH reaction was calculated.

Typically crowding is expected, conceptually, to reduce the amount of steric interactions by favoring product formation. However, our results in a buffer, Ficoll−70 (200 g/L), and Ficoll−70 (400 g/L) environment, show that the product formation continually decreased (looking at dissociation constant). This observation is attributed to a reduced number of potential interactions that NADH and LDH have to form a complex in a highly crowded environment. Interestingly, as the crowding agent increases drastically in size from 70,000 Da to 400,000 Da, the dissociation constant decreases substantially. Because this size difference of the crowding agent, it is apparent that LDH (and NADH) are able to navigate through Ficoll−400 easier than Ficoll−70, leading to more product formation. This is consistent with an increased buffer-like space among larger crowding agents (i.e. Ficoll−400). Previous studies have shown that small macromolecules can increase

enzymatic activity through containment (caging), while macromolecular size effects of crowding agents usually dominates.[35] Here, Ficoll−70 is much smaller than Ficoll−400 and therefore is expected to reduce the dissociation constant through increased caging effects. However, our results indicate enhanced association in Ficoll−400. This previous study is consistent with our interpretation that the size of the crowding agents dominates. At lower concentrations of Ficoll−70, where NADH and LDH could diffuse more easily, Ficoll−70 could potentially have a lower dissociation constant than Ficoll−400. This size effect of crowding will be explored further in section 5.4 (dextran).

5.2 Apparent Weak Interactions of NADH with Ficoll

Interestingly, Ficoll crowding should have negligible effect on the rotational time of free NADH (unlike glycerol), considering that Ficoll is a neutral (inert) polymer with no effects on the viscosity of the buffer-like environment surrounding the excluded volumes.[2] However the rotational time ($\boldsymbol{\varphi}$) of the free NADH in Ficoll−70 enriched buffers has two different, distinct rotational times. These two distinct rotational times of pure NADH even show a slight *associated* anisotropy characteristic (Figure 5.2), compared to a biexponential NADH decay in *Tris* and glycerol-enriched buffer. One of these rotational times ($\boldsymbol{\varphi}_1$) is comparable to a buffered environment (expected from literature, ~0.1 ns).[11] However, the second rotational time ($\boldsymbol{\varphi}_2$) is significantly larger that suggests some weak interactions with Ficoll−70 (>3 ns). This observation is not unique to Ficoll−70 and is also present in Ficoll−400. Attention should be drawn back to homogenous crowding to highlight that this longer rotational time seen in Ficoll is not

seen in glycerol-enriched or a buffered environment. While time-resolved anisotropy of [NADH]:[LDH] mixture (2:1 to 32:1) exhibit associated anisotropy profiles in Ficoll crowded environment, the decay features seem different from that in pure *Tris* buffer as well as homogeneously viscous environment using glycerol. For example, the fractional amplitude (β_2) of the slow-rotating species, i.e., LDH$(NADH)_n$ complex, starts relatively low at 32:1 and increases gradually with the relative LDH concentration. This very observable anisotropy difference between homogeneous and heterogeneous crowding anisotropy curves is shown in Figure 5.2.

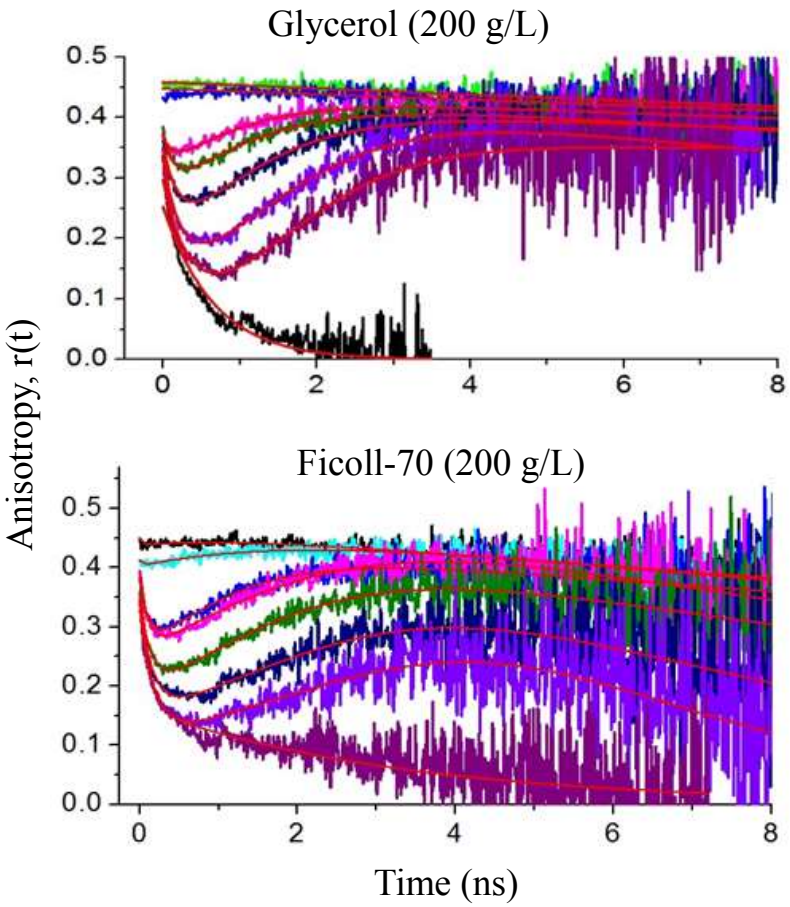

Figure 5.2: The associated anisotropy curves of NADH-LDH mixtures comparing both glycerol and Ficoll enriched buffers. The rotational times of the bound NADH (later times). The fast rotational time of the bound NADH component could be weak interactions.

With this caveat of an apparent weak interaction of Ficoll with NADH-LDH, extra precaution for assignment of free and enzyme-bound NADH was taken into account. If NADH was actually bound to Ficoll, and not LDH, this could influence the calculations for dissociation constant (K_d). This weak interaction claim can also be seen in our steady-state anisotropy measurements (Figure 5.3). At higher ratio of LDH:NADH (1:1 and 2:1) most of the NADH in the solution should be bound to LDH, where at more dilute LDH concentration (32:1 and 1:0), most of the NADH should be free. Because NADH is very

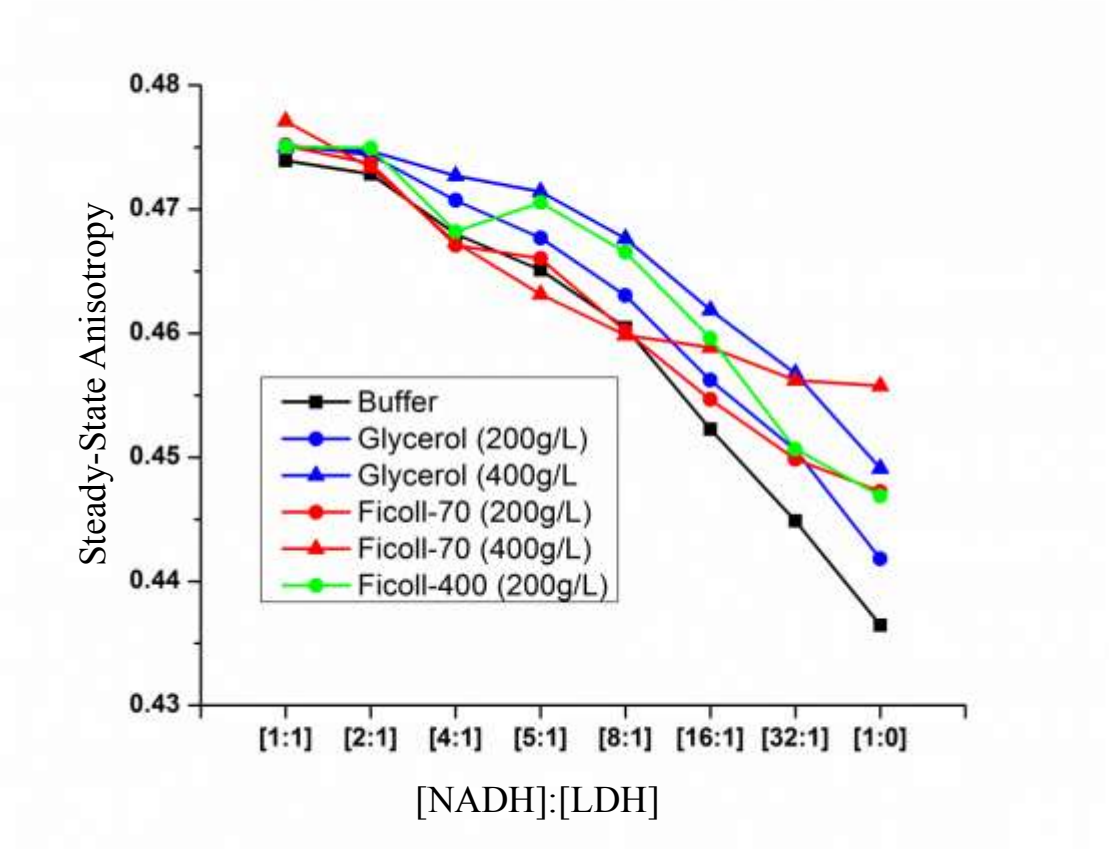

Figure 5.3: Steady-state anisotropy derived from time-resolved anisotropy data. Each plot shows a different ratio of [NADH]:[LDH] in various crowded environments that were shown previously.

small, weak interactions with Ficoll should be very noticeable by a larger rotational time. Because LDH is very large, a weak interaction with Ficoll should not be observed. Notice, at higher concentrations of LDH, the angle between the exciting and emitting dipole (r_{ss}) for buffer and crowding agents (homogenous and heterogeneous) are very similar. When more NADH is unbound, these anisotropy lines start to deviate. The Ficoll−70 line (400 g/L) shows the most abrupt change at these lower [LDH] solutions. Ficoll−70 at 200 g/L does show some deviation, but not as abrupt. This makes sense in that NADH has the potential to interact with more Ficoll in a more concentrated Ficoll sample, to increase the probability of weak interactions. Additionally, it is important to

note that glycerol does not deviate at these lower concentrations of LDH, suggesting no interactions in homogenous environments. These deviations further support the idea of weak interactions of NADH binding to Ficoll and need to be considered for data analysis.

5.3 Accounting for Weak Interactions with Heterogeneous Crowding

For (2P)-fluorescence lifetime measurements, free NADH showed characteristics of weak interactions with Ficoll-70 through a third fractional component (α_3) and a third lifetime component (τ_3) that is longer than expected. Because there is no LDH in these samples (1:0), and this third component does not exist in *Tris* or glycerol-enrich buffer, this third component must be attributed to NADH binding to Ficoll. This third fitting parameter can be seen in Table 5.1 (**bolded**):

Table 5.1: A representative table of the (2P)-fluorescence lifetime parameters for ficoll−70 to show weak interactions.

Environment: [NADH]:[LDH]	α_1	τ_1 (ns)	α_2	τ_2 (ns)	α_3	τ_3 (ns)	f_b (%)	K_d (μM)
Ficoll-Enriched: (200g/L)								0.103 ±
1:1	0.81	1.085	0.191	2.824	−−	−−	1	0.03063
2:1	0.79	1.065	0.208	2.603	−−	−−	1	
4:1	0.59	0.433	0.352	1.147	0.061	2.957	0.69	
5:1	0.51	0.561	0.439	1.416	0.048	3.369	0.72	
8:1	0.51	0.579	0.442	1.411	0.051	3.289	0.72	
16:1	0.71	0.365	0.262	0.832	0.024	3.150	0.09	
32:1	0.69	0.367	0.275	0.875	0.037	2.710	0.13	
1:0	0.68	0.343	0.31	0.695	**0.009**	3.609	0	

This third component of free NADH, although very small (0.9%), was used to normalize the α_3, in the rest of the samples (32:1, 16:1, 8:1, 5:1, 4:1, 2:1, 1:1). For 1:1 concentration ratio, we assigned that all NADH were bound to LDH, which is consistent with the number of binding sites of LDH. Since all of these samples have the same concentration of the crowding agent, NADH in the samples, should experience the same amount of weak interactions. The associated anisotropy parameters were corrected in the same way to account for weak interactions. The only difference is that lifetime can be fit to 3 components, where anisotropy was only resolved to 2. Figure 5.1 above shows agreement between the estimated dissociation constant using fluorescent lifetime and anisotropy in heterogeneous Ficoll based crowding. The fitting parameters for Ficoll using lifetime and anisotropy can be found in the appendix 1.1 and 1.2. Crowding has typically been studied in larger systems to show the effects of crowding on dimerization[37], protein folding[37], and enzyme activity[37]. However, more small-molecule studies are being published and it has been shown recently that small molecule interactions with horseradish peroxidase of two different substrates are much more affected by crowding than traditional large protein-protein aggregation and protein folding studies.[37] That study found that small molecules are more sensitive to crowding because of weak interactions with dextran and polyethylene glycol (PEG).[37] In addition, they found that these weak interactions will also slow down enzymatic activity.[37]

5.4 Shape dependency of Heterogeneous Crowding

Because the inside of a cell has many different sizes and shapes of macromolecules, similar measurements were carried out in dextran−6, dextran−70, and dextran−150 kDa in a buffered solution to further investigate the relationship of macromolecular size as well as shape effects on NADH-LDH binding kinetics. Like Ficoll, dextran is known to be inert and should not interact with our NADH-LDH system (although our data showed weak interactions).[35, 38] While Ficoll is known to be a hard sphere model of macromolecule crowding, dextran has a cylindrical shape.[35, 39]A comparison of dextran−70 and Ficoll−70 (same size, but different shape) should, in principle, reveal how the shape might affect the binding kinetics. Similarly, dextran−6, 70, and 150 kDa will further be used to show the size dependency of a crowding agent on kinetics, much like Ficoll−70 and Ficoll−400, but of a different shape and smaller sizes. Our results of estimated dissociation constant are shown (Figure 5.4) below:

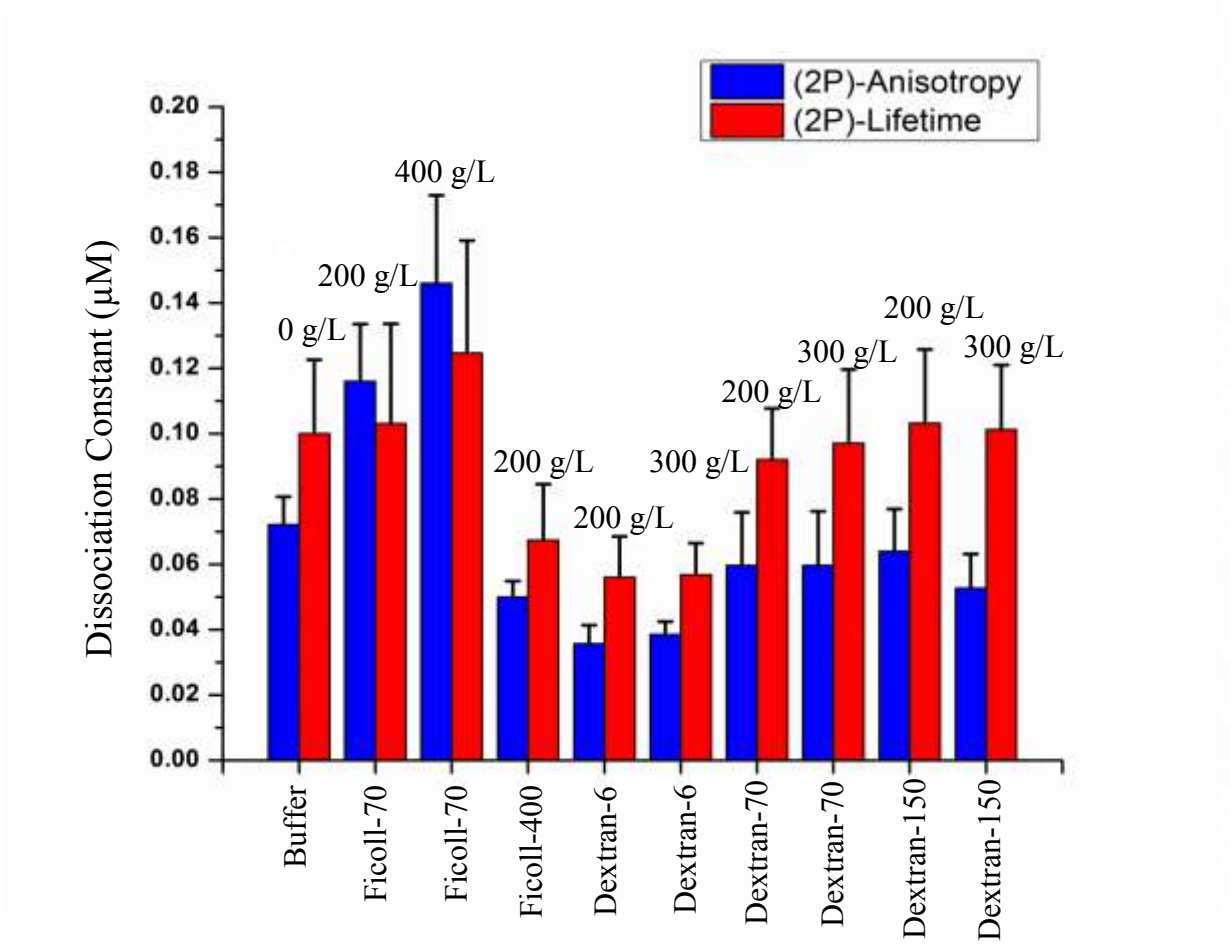

Figure 5.4: The dissociation constant (K_d) of NADH-LDH interactions are sensitive to concentration, shape, and size of crowding agent. Using both the time-resolved fluorescence and associated anisotropy curves, the corresponding dissociation constant of NADH-LDH reaction was calculated.

Similarly to Ficoll, dextran was also found to have some apparent weak interactions with NADH and LDH. The same longer rotational times (and third component with a longer lifetime) in free NADH samples (1:0) were revealed, and these weak interactions components were normalized in the same way as Ficoll. The observed longer rotational times can be seen in the appendix (1.1 and 1.2) where the full tables of fitting parameters can be found. In Figure 5.4, dextran−6 behaves similarly to glycerol and Ficoll−400, in that the product formation is favored (smaller dissociation constant). These results

highlight the idea that despite NADH and LDH having to navigate a lot of many small molecules (dextran−6) to bind, small molecules are better able to increase enzymatic activity through caging. The smaller crowding molecules are better able to conform to the enzyme more efficiently to prohibit dissociation to a greater degree. Furthermore, from dextran−6 to dextran−70 to dextran−150, the dissociation constants increase with increasing crowder size. These results could be due to a mixture of a decreased caging effect, or an increased excluded volume effect that prevents binding that we saw from Ficoll−70 to Ficoll−400. Comparing the shape of crowding agents is relatively new, and very limited amount of literature is currently available. With the same molecular weight (Ficoll−70 and dextran−70), dextran−70 has a considerably lower dissociation constant which suggests a favored product formation. Because dextran is known to behave as a cylinder, there should be a considerable amount of weak interactions present and should be explored. Shown in appendix 1.1 and 1.2, dextran does show a higher percent of free NADH bound to dextran compared to Ficoll molecules. On the other hand, Ficoll molecules are modeled as a more compact sphere that should have less weak interactions. Because of a larger surface area, dextran has the potential to have a smaller apparent volume in solution, leading to a higher product formation.

5.5 Conclusion of Solution Studies

Our results show that the observed dissociation constant of LDH$(NADH)_n$ complex decreases with increased glycerol concentration (i.e., the viscosity of this homogeneous environment) as compared with that in *Tris* buffer. This suggest that the viscous glycerol enriched buffer may stabilize the LDH$(NADH)_n$ complex formation. In other words, this will indicate the enhanced association constant (K_{eq}) between LDH and NADH in a viscous, homogeneous environment. However, perhaps the way we mix NADH and LDH in different environment may help. For example, mixing our product using gentle vortex prior to measurements may facilitate potential encounters between LDH and NADH. Interestingly, the dissociation constant of LDH$(NADH)_n$ complex in *Tris* buffer enriched with 200 g/L of Ficoll−70 is significantly larger than that of pure buffer at room temperature. This means that the corresponding association constant in the presence of 200-g/L Ficoll−70 is smaller than that of homogeneous, pure buffer. As we increased the Ficoll-70 concentration to 400 g/L, the dissociation (association) constant increased (decreased) as compared with 200 g/L. The observed NADH-LDH kinetics suggests that the excluded volumes occupied by the Ficoll−70 in a heterogeneous environment exhibit different trends as compared with the viscous, homogeneous environment. We attribute this observation (NADH and LDH in this case) to water-like cages made up by excluded volumes occupied by heterogeneous crowding agents.

Chapter 6: DIC and Confocal Imaging to Address Cellular Morphology

6.1 Rationale

Prior to 2P-FLIM and anisotropy studies of NADH in living cells, we carried out confocal and DIC microscopy on C3H10 cells in culture to assess cellular morphology.

6.2 Identification of Healthy and Stressed Cells

It is important that we are able to visually identify healthy cells from stressed cells. The purpose of these cellular studies is to measure the shift in NADH and enzyme-bound NADH due to metabolic manipulation, using non-invasive and quantitative measurements at the level for single cell diagnostics. These ratios must be compared to a healthy cell at resting conditions. If stressed cells are chosen for FLIM and anisotropy measurements, no change may be observed when drugs are introduced, or these results could be skewed. It is known that apoptotic cells display a plasma membrane morphology called "blebbing".[10, 40] This blebbing of a stressed cell can be seen in Figure 6.1 by the rounding bubbles of the plasma membrane, and is often the hallmark of apoptosis.[10, 41] However, healthy cultured cells can be found to bleb during certain parts of the cell cycle as well.[41] In addition, the rounding of cells can play a role in cell movement.[41] In this case shown, these "stressed" cells were found within a cell plate that was overall very healthy. As a precaution, whether these blebbing cells were going through stages of mitosis, or were stressed, those cells were avoided in our analysis to avoid any confounding results.

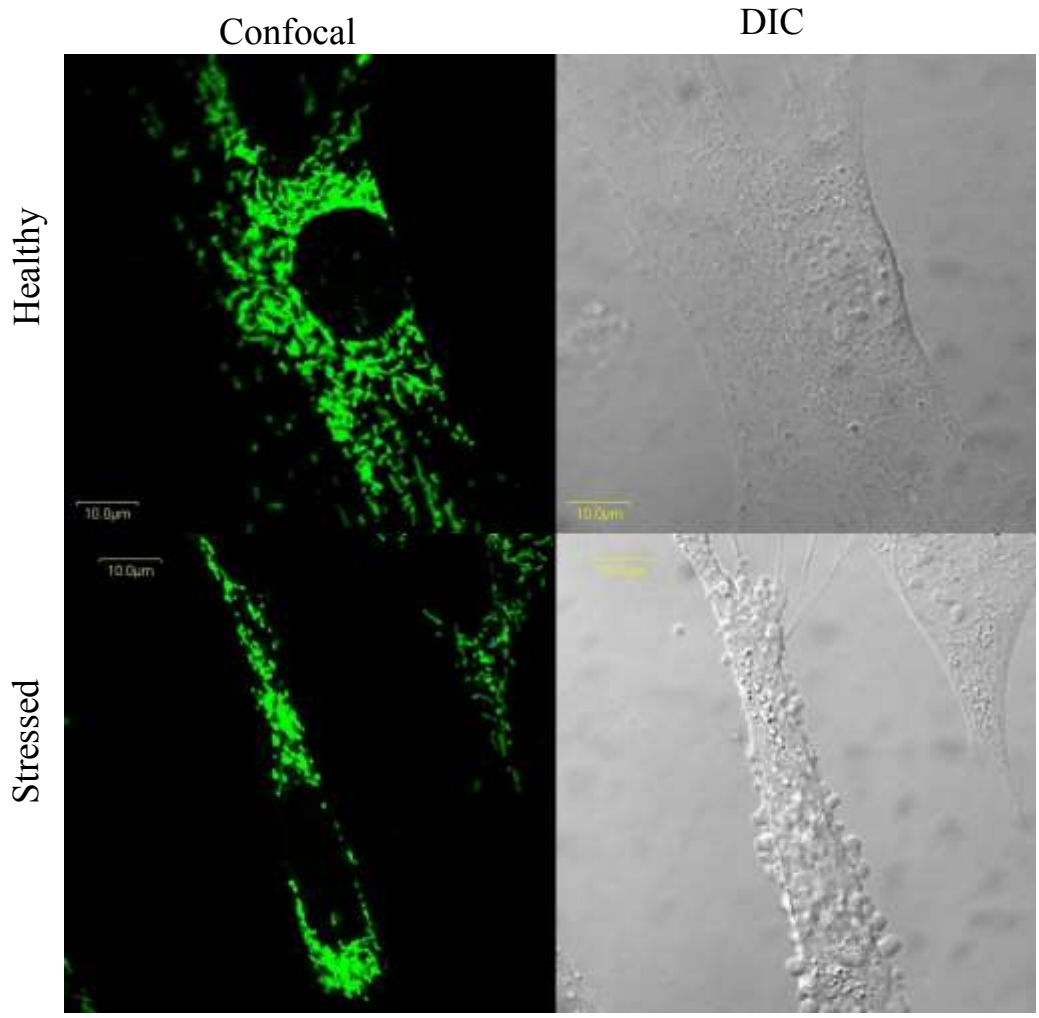

Figure 6.1: Identification of a healthy and stressed C3H10 fibroblast cell using DIC and confocal imaging. Rhodamine 123 was used to as the green mitochondrial stain shown here. Scale is shown as 10 µm and this was achieved by a zoom of 3.

6.3 Mitochondrial Morphology using Confocal Microscopy

In the materials and methods section, it was mentioned that two different mitochondrial dyes (Rhodamine 123 and MitoTracker Green FM) will be used to assess cell and mitochondrial morphology of C3H10 cells. It is advertised that MitoTracker Green FM has a fluorescence emission only when bound to the mitochondria. Furthermore, MitoTracker Green FM was advertised by the supplier as requiring no washing of the cell

after incubation (although this washing was still done three times as a precaution). Interestingly, MitoTracker had a large fluorescence background as if the fluorescent dye was even emitting in the extracellular matrix. We also used Rhodamine 123 as a mitochondrial marker and an enhanced contrast was observed. Figure 6.2 below highlights this difference.

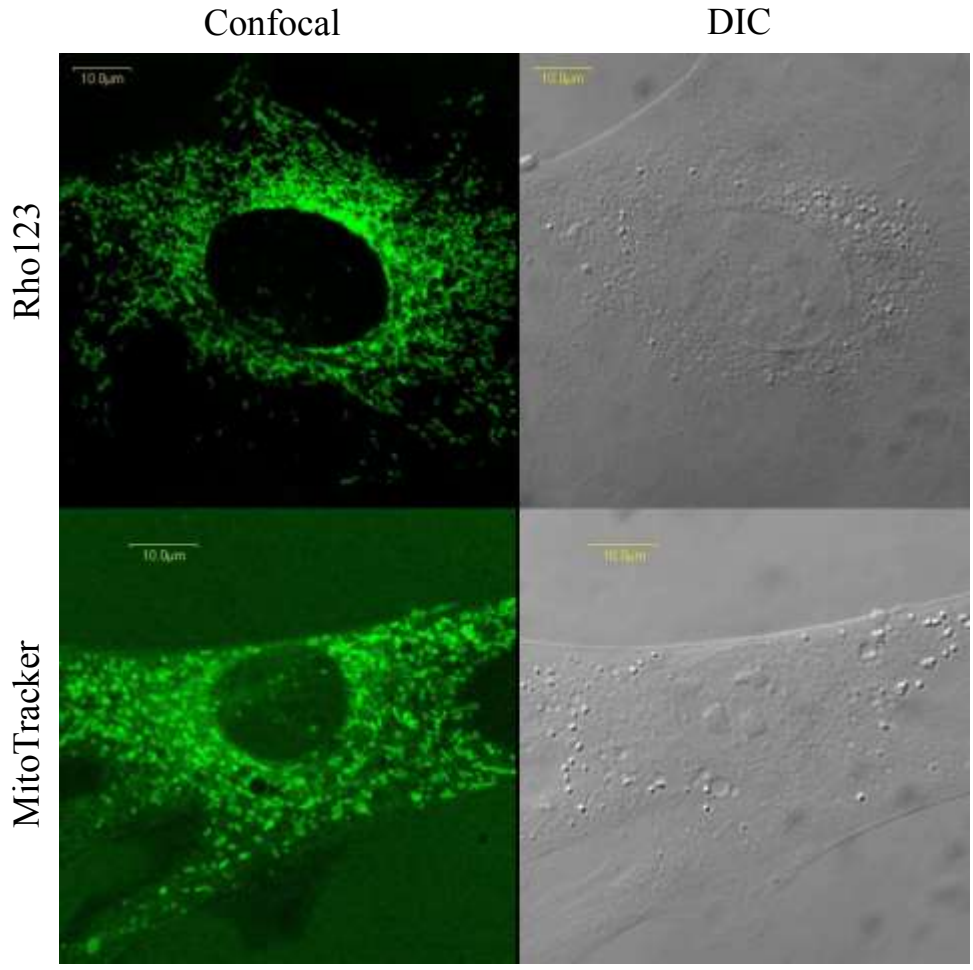

Figure 6.2: Confocal and DIC image comparing the contrast and background fluorescence of Rhodamine 123 and MitoTracker Green FM. Scale is shown as 10 µm and this was achieved by a zoom of 3.

6.4 Time-Lapse Confocal Imaging of Resting Cells in Culture

FLIM and anisotropy methods generally take 3-5 minutes for data collection. In addition, we may want to image more than one cell within the dish. Between set up of instrumentation, acquisition time of data collection, and imaging more than one cell, the cells could be exposed to the air for more than 30 minutes. First, it is necessary to make sure that the cells can withstand our laser power for 3-5 minutes at a minimum movement, for FLIM and anisotropy measurements, by assessing the morphology changes of the cell. Second, it is important to show how long our cells can remain healthy outside of the incubator (37°C and 5% CO_2). To address these issues, C3H10 fibroblast cells were exposed to a laser-scanning source for 1 hour, with a frame per minute. Figure 6.3 shows 5 frames of the 60 images (0, 15, 30, 45, and 60 minutes) collected for this experiment. Looking at the corresponding DIC images, the cells show no signs of stress, apoptosis, or changed morphology after one hour, besides minor cell movement. Confocal imaging show significant decrease in Rhodamine 123 fluorescence signal, even after 15 minutes. This decreased fluorescence doesn't necessarily mean that the mitochondria are becoming depolarized and losing the stain, but the excess excitation is photobleaching the fluorophore. When we move to imaging intrinsic NADH, photobleaching will not be a problem due to short acquisition times of FLIM (3-5 minutes) and anisotropy methods.

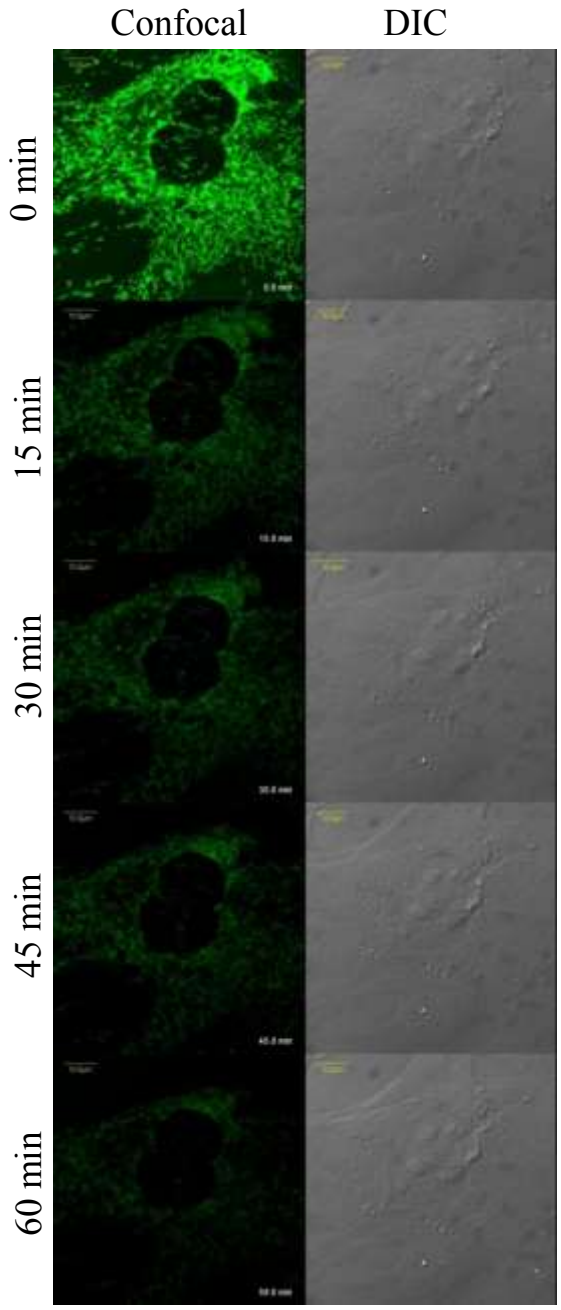

Figure 6.3: Healthy C3H10 cells imaged using confocal and DIC methods over one hour. Decrease in fluorescence is due to photobleaching because of extended exposure to excitation source. No visible signs of apoptosis are seen after one hour. Scale is shown as 10 μm and this was achieved by a zoom of 3.

6.5 Time-Lapse Confocal Imaging of Culture Cells under Rotenone Treatment

Inhibition of complex I in oxidative phosphorylation pathways, which prevents the oxidation of NADH (fluorescent) to $NADH^+$ (non-fluorescent), has been extensively investigated within the context of apoptosis and cell death.[42] It is generally accepted that the mitochondria are the main regulator of apoptosis in living cells.[42] Rotenone is an inhibitor of complex I of oxidative phosphorylation.[20] If, rotenone prevents the oxidation of NADH, we should expect a measurable increase in free NADH. Previous studies using rotenone treatment of cells at a concentration of 1-10 μM did study changes in ATP levels, hydrogen peroxide production, superoxide production, DNA fragmentation, and measurement of apoptosis.[42-43] We carried out confocal and DIC imaging of C3H10 cells in culture with treatment of 1 μM rotenone for monitoring any morphology changes of cells over one hour. Prior to time-lapse imaging, the normal complete medium was removed and replaced with new medium; rotenone (1 or 10 μM) was then quickly added. After addition of new rotenone-containing media, confocal and DIC imaging were promptly acquired. These results are summarized in Figure 6.4 below.

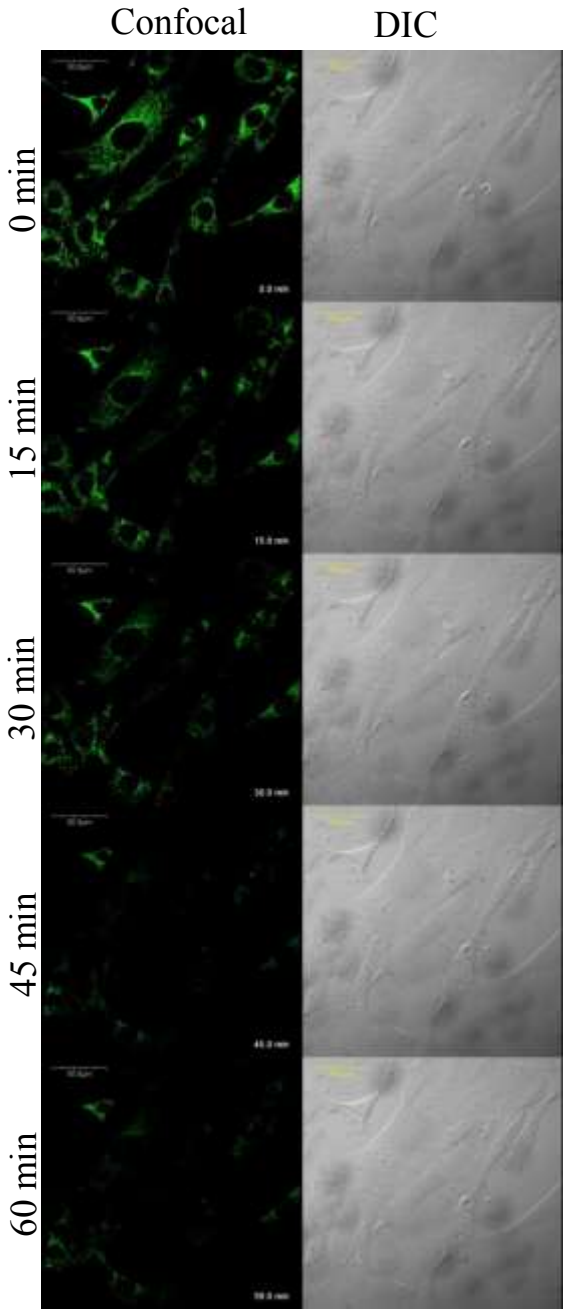

Figure 6.4: Healthy C3H10 cells imaged using confocal and DIC methods over one hour. Rotenone (1 µM) was added to dish at time zero. Decrease in fluorescence is due to photobleaching because of extended exposure to excitation source. No visible signs of apoptosis are seen after one hour. Scale is shown as 50 µm, achieved by a zoom of 1.

At 1 μM of rotenone treatment after 1 hour of incubation, there were no visible signs of apoptosis or change in cell morphology. Just because there are no visible signs of apoptosis or blebbing does not mean there aren't change on the molecular level of mitochondrial activities. A higher concentration of rotenone (10 μM) was also used to further address cellular stress and morphology changes. It is believed that incubation with 10 μM of rotenone will induce visible signs of apoptosis to verify what is reported in literature assuming C3H10 cells will respond the same way. Figure 6.5 below highlights this morphology change through the yellow squares, where the most change happens (0 and 60 minutes). However, we only saw a slight retraction of the cells. This same concentration of rotenone will also be further addressed using FLIM and anisotropy methods to elucidate the shift in free and enzyme-bound NADH.

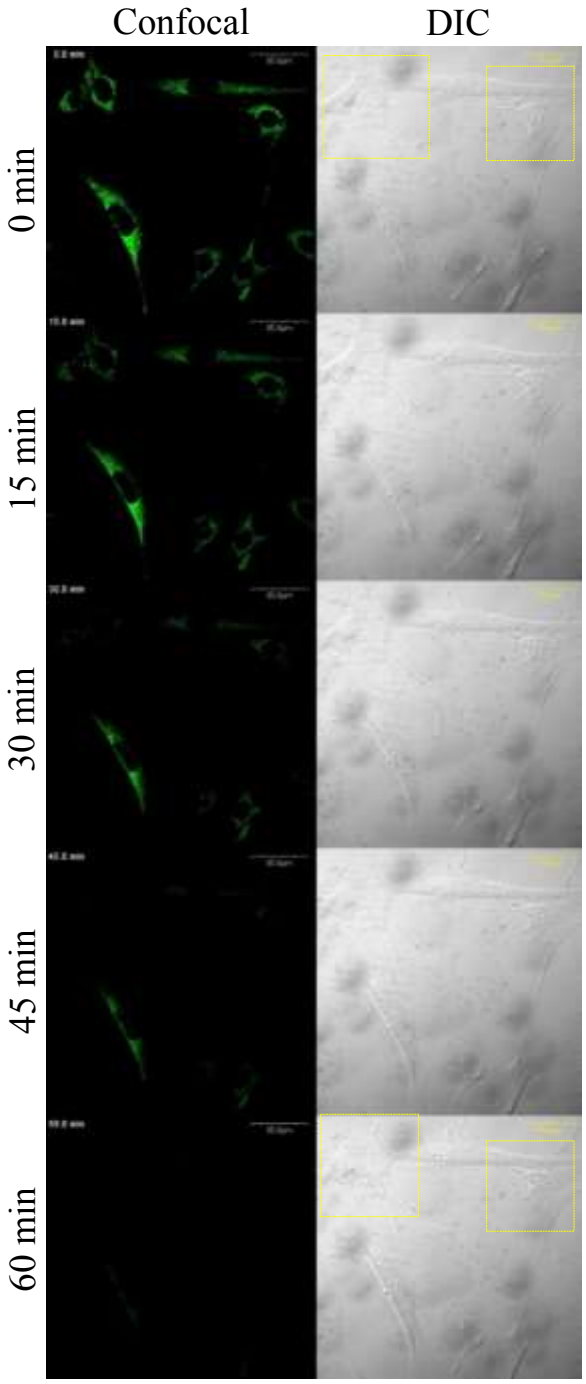

Figure 6.5: Healthy C3H10 cells imaged using confocal and DIC methods over one hour. Rotenone (10 µM) was added to dish at time zero. Decrease in fluorescence is due to photobleaching because of extended exposure to excitation source. Visible signs of apoptosis are seen after one hour, highlighted by yellow boxes. Scale is shown as 50 µm and this was achieved by a zoom of 1.

Chapter 7: (2P)-FLIM and (2P)-Anisotropy measurements to Address Free and Enzyme-bound NADH

7.1 Rationale

Living cells are crowded with large biological macromolecules and organelles.[1] To complement our studies in biomimetic environments (chapters 4 and 5), we focus here on live cultured cells using cellular NADH and a number of associated enzymes under both resting and rotenone-treated conditions. Intracellular NADH exists as a mixture of free and enzyme-bound populations at dynamic equilibrium throughout living cells, which will be imaged using fluorescence lifetime imaging for both quantitative and noninvasive assessment of cellular metabolism. We will use 2P-fluorescence lifetime imaging microscopy (FLIM) and 2P-fluorescence anisotropy of intrinsic NADH in cultured mouse embryonic cells (C3H10) under both resting conditions and metabolic-manipulation (mitochondrial electron transport chain). FLIM of the native NADH in resting (healthy) cells will serve as a reference point to calculate the fraction of free and enzyme-bound NADH in different cell compartments. Using laser-scanning mode of time-resolved anisotropy of cellular NADH will also enable us to show that NADH-enzyme kinetics exists as a dynamic equilibrium. The outcome of these cell studies will then be compared with our controlled solution studies. Comparative assessment of the binding kinetics with the same cell line under perturbed metabolic pathway and mitochondrial anomalies using rotenone will be a critical step towards quantitative, noninvasive diagnostics at the single cell level. Anisotropy and FLIM measurements of cellular NADH will be used to

examine whether metabolic manipulation (using rotenone as Complex I inhibitor) shifts the equilibrium dynamics of NADH-enzyme binding. Typically measurements to monitor mitochondrial function (or anomalies) include ATP measurements, superoxide changes, DNA fragmentation, NADH ratios, and respiration changes. These measurements use cell lysates, introduction of exogenous fluorophores, and flow cytometry.[42] Measurements using endogenous NADH are more limited, but rather informative due to the fact that cells remain intact and healthy with morphological context.

7.2 Two-Photon (2P) Fluorescence Lifetime Measurements (FLIM) of Resting C3H10 Cells

As a reference point, before rotenone treatment, healthy fibroblast cells were measured using (2P)-FLIM to elucidate the location of free and enzyme-bound NADH with spatial or morphological context. Furthermore, the fraction of enzyme-bound NADH can be calculated using 2P-FLIM images. Figure 7.1 below shows a typical (2P)-intensity, (2P)-FLIM, and the corresponding DIC image. These DIC images before and after 2P-FLIM were used as a control to ensure negligible photodamage or laser-induced stress during 2P-FLIM. The 2P-intensity is simply the integrated area under each fluorescence lifetime per pixel (binning = 4) to show where the most fluorescence is concentrated in apparent mitochondria. In the FLIM image, 256 X 256 pixels were used during laser-scanning, where each pixel has a unique lifetime (color). Each lifetime can be compared to the color code shown (0.4 to 2.0 ns). The FLIM image was fit to only 2 components (free and enzyme-bound NADH). However, these color-coded FLIM images reflect the average

lifetime per pixel. With these parameters, a calculated enzyme-bound NADH fraction can be calculated in mitochondria, cytosol, and nuclear regions. Previous studies, using non-invasive anisotropy techniques have shown that Hs578Bst cells have an enzyme-bound fraction of 0.82 ± 0.08.[9] Additionally, similar (2P)-fluorescence lifetime measurements were done on neural cells derived from PC12 cells, where a calculated fraction bound (NADH) of untreated cells was 0.85 (p-value < 0.001).[44] The DIC image reveals healthy C3H10 cells prior to imaging with no apparent stress.

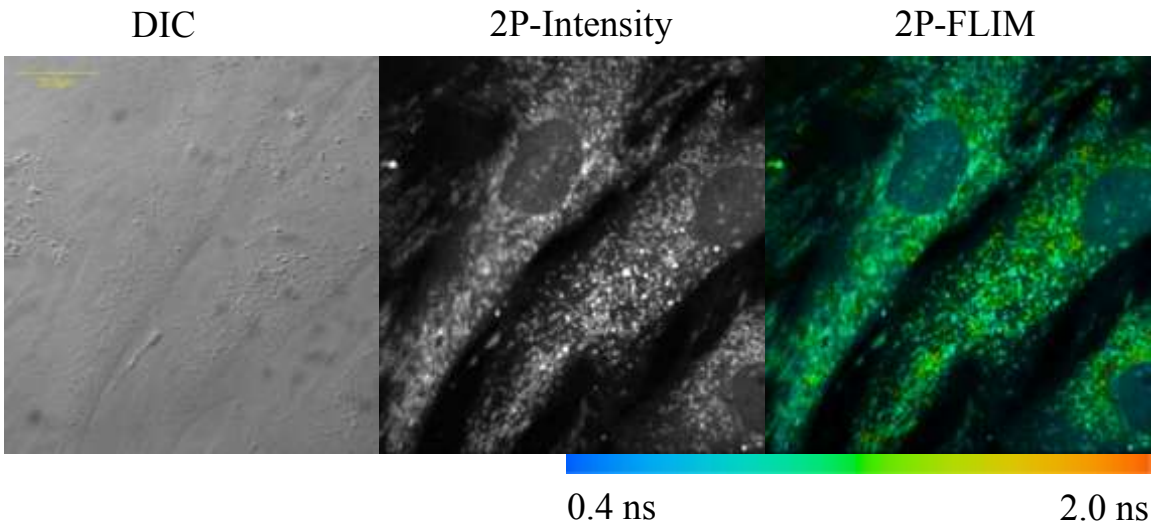

Figure 7.1: FLIM and DIC of resting C3H10 fibroblast cell imaged under resting conditions using (2P)-FLIM. The intensity is simply the integration of the fluorescence lifetime at each pixel. Each pixel (256X256) has a unique fluorescence lifetime decay that was scanned, and corresponds to a fluorescence lifetime seen in the legend below (0.4 to 2.0 ns). FLIM was measured using a 76 MHz laser pulse (730 nm excitation), no magic angle detection, 1.2 NA water immersion objective, a zoom of 3 (10 µm scale), and an optical density of 0.6. Each acquisition time was 300 seconds.

The 2P-Intensity shows that most NADH (in mitochondria) is highly concentrated around the nucleus, which is not surprising due to the generation of ATP for nuclear processes. This NADH intensity is consistent with literature in that most NADH is said to be found in the mitochondria (~400 μM), some in the nucleus and cytosol (100 μM), and even some in the extracellular space (~ 1 μM).[45] Because NADH is sensitive to enzyme-binding, pH, and viscosity, 2P-FLIM images can reveal diverse microenvironments and structures (binding) of NADH which is compartmentalized within a cell, and even from cell to cell. Each cell consistently has a nucleus that is dominated by a fluorescence lifetime of 0.4 ns (blue on scale) that is indicative of free NADH. This NADH pool in the nucleus, is attributed to interactions with proteins that regulate transcription, and NADH is associated with regulating histone acetylation.[46] Additionally, some of this NADH in the nucleus could be due to out-of-focus fluorescence from either the top or bottom of the nucleus. Most NADH around the nucleus (attributed to apparent mitochondrial NADH), is dominated by a long lifetime of ~1 ns (green). As one can see, not all of the cells are equal, despite all healthy-looking morphology. The second to the bottom cell has a very different distribution of mitochondria and much longer lifetimes (more orange/red). Additionally, this same cell does not have a high concentration of NADH around the nucleus like the others. The apparent mitochondria in the FLIM images seem less connected as shown in Rho123-stained cells using confocal imaging. This might be attributed to the mitochondrial movement during the 300 second data acquisition. Another possibility is laser-induced fragmentation of mitochondria. However, this speculative argument requires further investigation. These observations will be important

to recognize changes in rotenone-treated cells.

7.3 Time-Lapse 2P-FLIM of Rotenone Treated Cells in Culture

Inhibition of complex I in oxidative phosphorylation pathways prevents the oxidation of NADH (fluorescence) to $NADH^+$ (non-fluorescent). [42] With this in mind, we hypothesize cells treated with rotenone should have a build-up of free NADH in the mitochondria over time, leading to a higher fluorescence intensity. Here, we treat C3H10 cells with 10 μM of rotenone and we image the same cells at time 0, 30, and 60 minutes (limited images to decrease photo-bleaching and stress to cells). Small movement of the cells was observed due to cell drifting or cell movement while removing and adding rotenone treated media during 2P-FLIM imaging. Figure 7.2 shows the results of cells treated with rotenone. At time zero, typical healthy cells are seen, where rotenone treatment has not affected the cells (at least it is not apparent using 0.4-2.0 ns color code range). A high concentration of mitochondria is seen around the nucleus as in the previous experiment with no rotenone treatment. Additionally, the nucleus is populated with what looks like free NADH (0.4 ns) as seen before. Over time, from 0 to 30 to 60 minutes of rotenone exposure, the mitochondria become large, rounded, and have a higher fluorescent intensity (2P-intensity image). Furthermore, it seems that the nucleus loses free NADH (0.4 ns) and becomes less fluorescent. This NADH from the nucleus could be building up in the mitochondria due to inhibition of Complex I by rotenone. Due to the increased intensity of the mitochondria, this NADH fluorescence in the nucleus could be also be reduced in comparison. Interestingly, the cells treated with rotenone also display larger

fluorescent lifetimes in the cytosol (shift to orange/red colors). This shift in lifetime could be due to shifting metabolic priority to glycolysis (Lactate dehydrogenase or Malate Dehydrogenase bound) from oxidative phosphorylation (previously complex I bound). We observed no laser-induced stress of the cells during these FLIM images. Currently, we are reanalyzing these FLIM images using the spatial distribution of both the short lifetime (free NADH) and the long lifetime (bound NADH) in each image. Parallel analysis will also be conducted based on the amplitude fraction (i.e. population) of each decay component (species) per pixel. Importantly, we will quantify the concentration of NADH in the cytosol, mitochondria, and the nucleus. Finally, we will revisit the analysis using a different color code range. Our rationale is that 0.4-2.0 ns range may suppress minor changes of FLIM as a function of rotenone treatment. Additionally, as a control for the future, we plan to image the same cells at time 0, 30, and 60 minutes with no rotenone to ensure the cell's response to rotenone is actually to rotenone and not laser-induced stress.

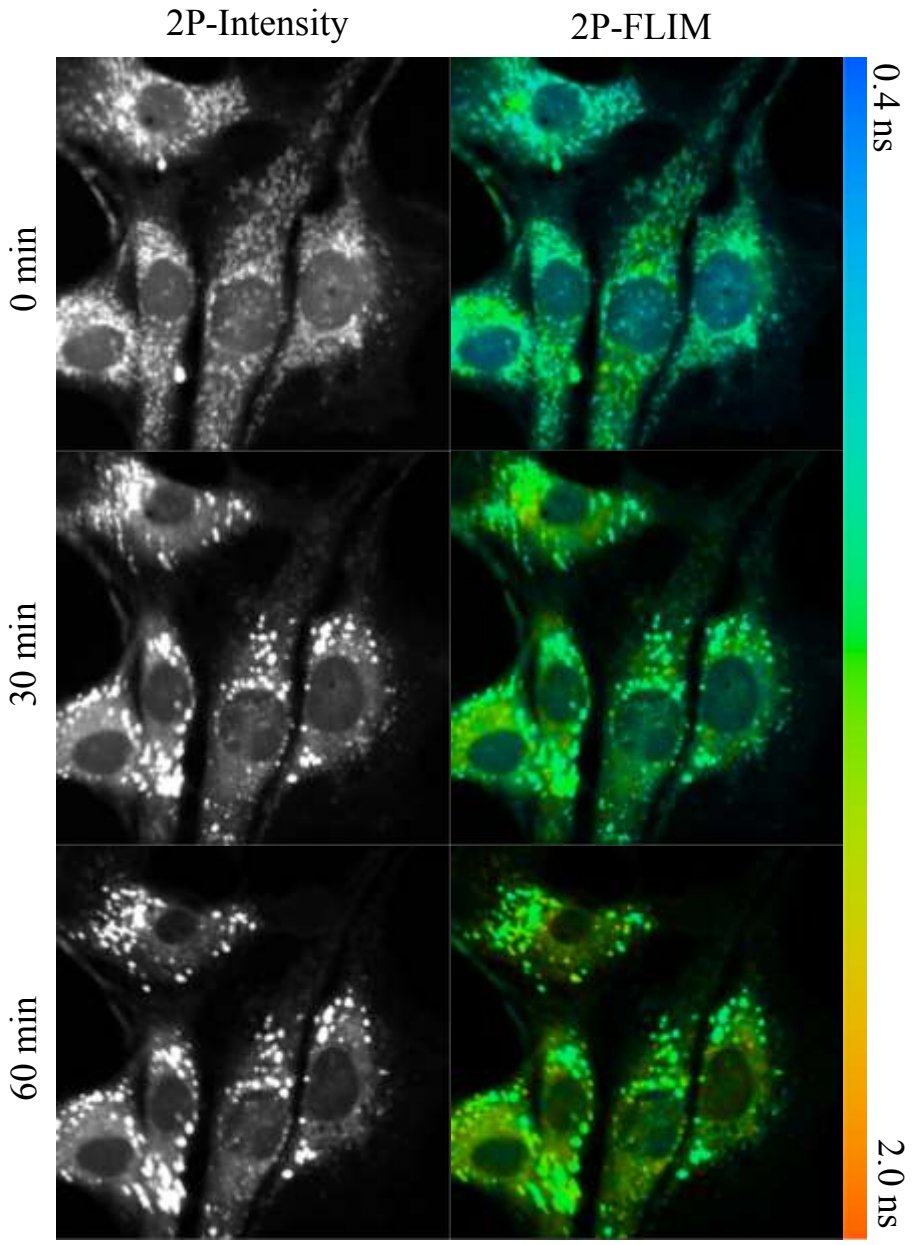

Figure 7.2: Results of C3H10 fibroblast cell imaged with10 µM rotenone for 0, 30, and 60 minutes of incubation using (2P)-FLIM. The intensity is simply the integration of the fluorescence lifetime at each pixel. Each pixel (256X256) has a unique fluorescence lifetime decay that was scanned, and corresponds to a fluorescence lifetime seen in the legend below (0.4 to 2.0 ns). FLIM was measured using a 76 MHz laser pulse (730 nm excitation), no magic angle detection, 1.2 NA water immersion objective, a zoom of 2.5, and 0.2 OD. Each acquisition time was 300 seconds.

7.4 (2P)-Fluorescence Anisotropy Measurements of Healthy C3H10 Cells

As a comparative method to calculate the ratio of free and enzyme-bound NADH, healthy resting C3H10 fibroblast cells were measured using time-resolved (2P)-associated anisotropy. In these measurements, the laser was scanned over the cells in the field of view and the average signal was resolved into parallel and perpendicular polarization to calculate 2P-anisotropy. A typical curve (Figure 7.3) shows the same associated anisotropy profile that was in our control solution studies using NADH and LDH titrations (fast and slow rotational times).

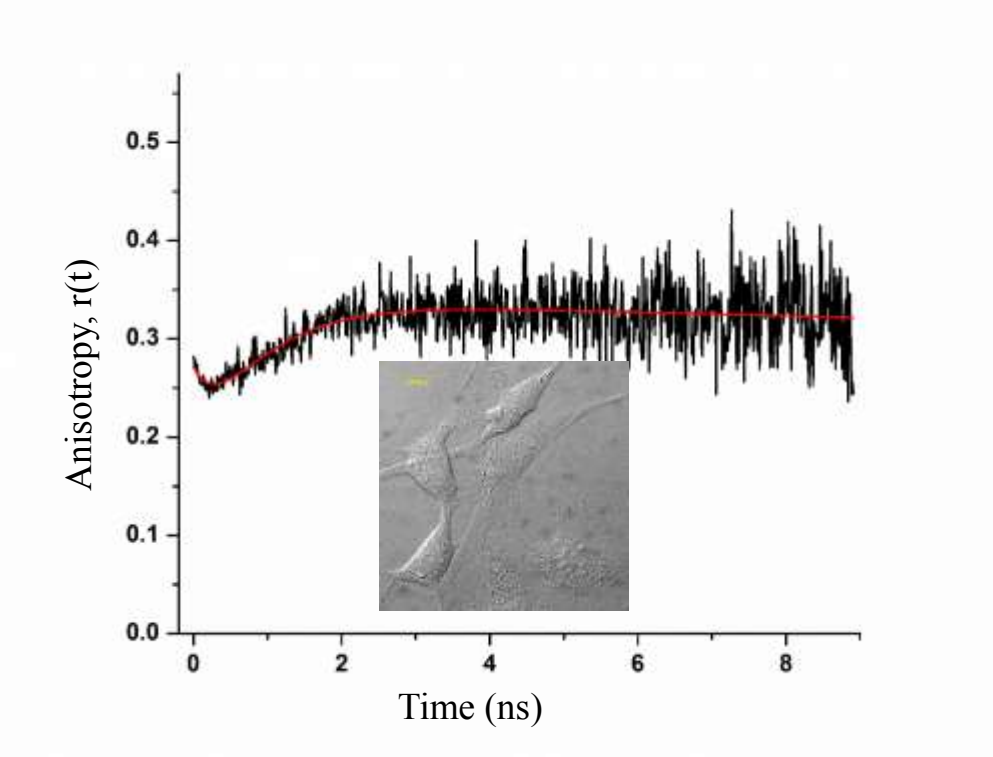

Figure 7.3: Time-resolved (2P)-Associated Anisotropy measurements of C3H10 fibroblast cells at resting conditions. Cells were excited at 730 nm (NADH excitation) at 4.2 MHz repetition rate of 630 mW laser intensity. A zoom of 2.5 was used, with an optical density of zero. Cells were imaged (DIC) after anisotropy measurements with no signs of further stress.

Keep in mind that the generated associated anisotropy curves (using NADH as a biomarker) in a cell are not just NADH and LDH. Rather, NADPH and NADH and their interactions with a myriad of enzymes can be present. In addition, LDH is not the only enzyme that NADH binds. These cellular associated anisotropy curves show the bulk NADH and NADPH and all of their respective enzymes. Figure 7.3 shows one representative associated anisotropy curve from resting C3H10 cells. The curve shown was used to calculate the free NADH component and an enzyme bound component. The cellular associated anisotropy curve was fit to equation 7, and the fraction bound was calculated using equation 9 (in a similar manner as in the solution studies). Four of these measurements were done on different cells (n=4), and very similar fraction NADH enzyme-bound numbers were found to be 0.47, 0.44, 0.33, and 0.44 (average of 0.42 ± 0.03). It is interesting how close these NADH bound calculations were despite 2P-FLIM revealing that cells in the same image (over 0.4 to 2.0 ns range) can compartmentalize NADH very differently. Comparing this to our solutions studies (chapters 4 and 5), the fraction bound of intercellular NADH is very similar to typical ratios between [16:1] and [8:1] NADH:LDH solution in a buffered environment. The measured rotational times of cellular NADH had a free and bound component of ~0.35 ns and a very large rotational time (> 1E6 ns) that is typical of large molecules that might be constrained by surrounding micro-environments inside the cell. Compared to a *Tris* buffered solution the typical rotational times of free and bound NADH were ~0.1 ns and ~50 ns. These increased rotational times make sense in that cells are a lot more complicated as compared with a buffered environment because cells are viscous, highly crowded, NADH

binds to various enzymes, and NADPH also exists.

7.5 Time-Lapse 2P-Anisotropy of Rotenone Treated Cells in Culture

As seen in 2P-FLIM, we treated cells with rotenone to inhibit complex I in oxidative phosphorylation pathways to prevent the oxidation of NADH. As opposed to FLIM, anisotropy measurement will not reveal spatial distribution of NADH within a cell. However, with anisotropy, we can reveal how the fraction population (α_i) of free and bound NADH changes with their respective fluorescent lifetime (τ_i) and rotational time (φ_i). Because of the results seen in FLIM, and the increase of fluorescence intensity (thought to be due to NADH not being oxidized) in mitochondria, we expect the free NADH component (α_1) to increase over time, with rotenone treatment. Figure 7.4 below shows the results of C3H10 cells treated with 10 µM of rotenone over 60 minutes (measurements taken at time 0, 30, and 60 minutes). The figure below shows the results at time zero and after one hour incubation. The corresponding DIC images shown were taken after anisotropy measurements to address cellular stress. The results at 30 minutes were the same as at one hour, so the former is not shown. At time zero, a typical associated anisotropy profile is observed that is comparable to the non-rotenone treated cells (NADH fraction bound of 0.44). After anisotropy measurements at time zero, the cell morphology is healthy. However, at 30 minutes and 60 minutes, all of the free NADH component is lost (α_1), and only a long rotational time is observed. These cells seem to be losing all of their NADH through their membranes. This anisotropy curve is analogous to fully bound [NADH]:[LDH] = 1:1 in the solution studies, where the

anisotropy curve fit to a single exponential decay (one rotational time and one fluorescence lifetime). The absence of the associated anisotropy profile observed after 60 minutes of incubation with rotenone suggests that under laser-induced cell damage/stress (Figure 7.4, DIC panel) the free NADH may be attributed to photobleaching and we are only with enzyme bound NADH that is constrained in its local cell environment. Additionally, the DIC image reveals rounding of the cell's nucleus; it is preparing for apoptosis. Although we used a low repetition rate laser source, due to the nature of anisotropy measurements (two detection channels for parallel and perpendicular), cells cannot handle multiple anisotropy measurements. To overcome this challenge, multiple other anisotropy measurements were taken of nearby cells to assess the treatment of rotenone. Interestingly, nearby cells treated with rotenone (10 μM) show the same fitting parameters as the non-treated cells with a NADH fraction bound of 0.43 and 0.44. So despite FLIM images showing different NADH allocation of rotenone treated cells (loss of NADH in nucleus, increased mitochondria fluorescence intensity, and a potential shift to glycolysis), cells seem to find a way to optimize NADH free/bound ratio, even though oxidative phosphorylation is halted. It is worth noting that even under laser scanning conditions used for anisotropy measurements, we observed some indication of laser-induced cell stress. While these measurements were carried out at 4.2 MHz pulses, the peak intensity of these pulses may be a bit too high. Currently, we are repeating these measurements under different cell confluence. Importantly, we saw no laser induced damage or stress during the FLIM images due to the significantly lower laser power.

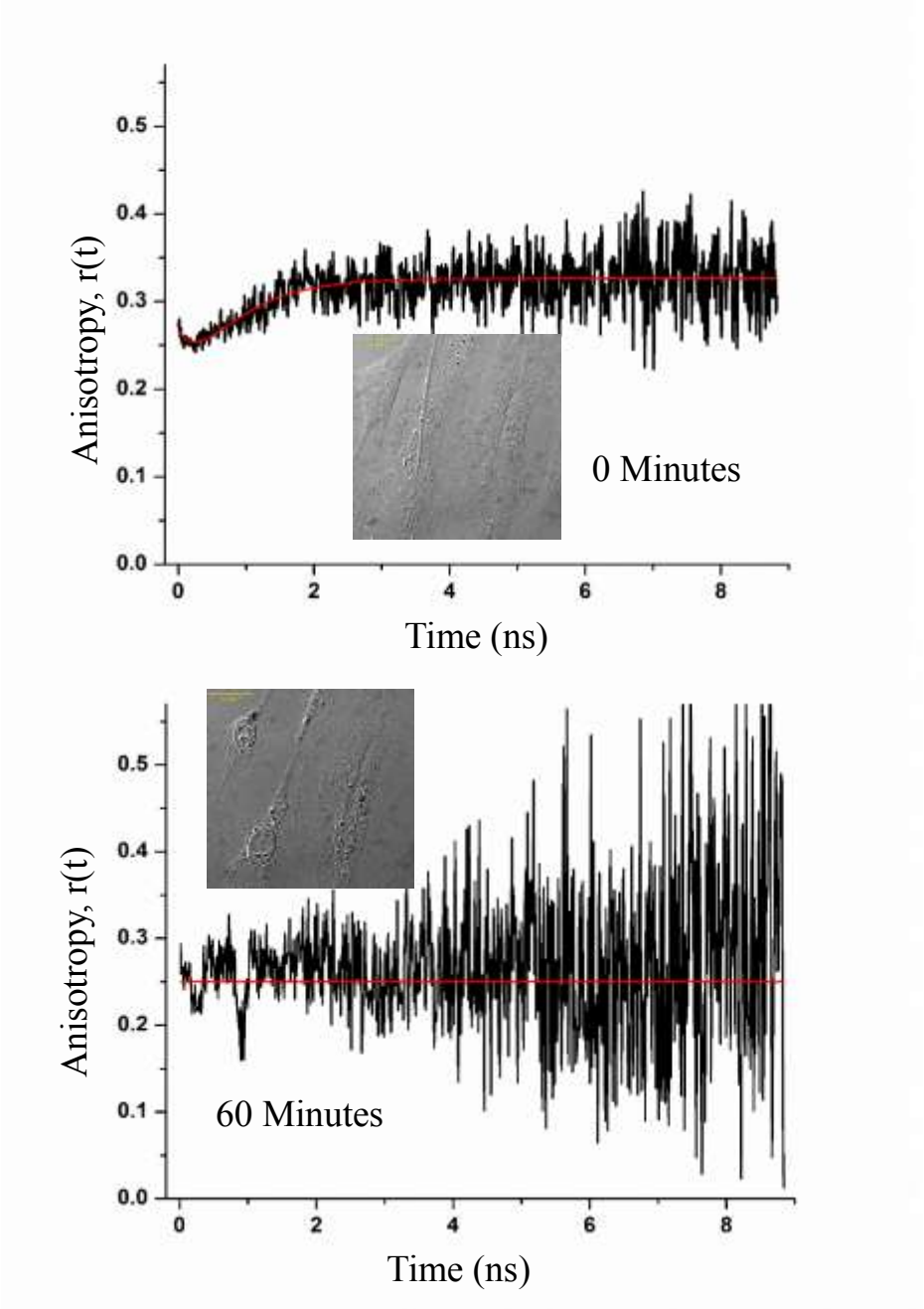

Figure 7.4: Time-resolved (2P)-Associated Anisotropy measurements of C3H10 fibroblast cells treated with 10 μM rotenone. Cells were measured at time 0, 30, and 60 minutes (30 minutes not shown here). Cells were excited at 730 nm (NADH excitation) at 4.2 MHz repetition rate of 630 mW laser intensity. A zoom of 2.5 was used, with an optical density of zero. Cells were imaged (DIC) after anisotropy measurements to show cell morphology

7.6 Summary

We investigated the sensitivity of cellular NADH interaction with dehydrogenases to metabolic manipulations. Our quantitative and non-invasive methodology complements the traditional biochemical and thermodynamics techniques without the destruction of live cells. Intracellular NADH also exists as a mixture of free and enzyme-bound populations at dynamic equilibrium throughout living cells, which can be imaged using fluorescence lifetime imaging for both quantitative and noninvasive assessment of cellular metabolism. 2P-fluorescence lifetime imaging microscopy (FLIM) and 2P-fluorescence anisotropy of intrinsic NADH were measured in cultured mouse embryonic cells under both resting conditions and metabolic-manipulation (mitochondrial electron transport chain). Inhibition of Complex I (using rotenone) in oxidative phosphorylation pathways prevents the oxidation of NADH (fluorescent) to $NADH^{+}$ (non-fluorescent).[42] With this in mind, we hypothesized cells treated with rotenone should have a build-up of free NADH in the mitochondria over time, leading to a higher fluorescence intensity. Despite FLIM images showing different NADH allocation of rotenone treated cells (loss of NADH in nucleus, increased mitochondria fluorescence intensity, and a potential shift to glycolysis), cells seem to find a way to optimize NADH free/bound ratio, even though oxidative phosphorylation is halted.

Bibliography

1. Minton, A. P., The influence of macromolecular crowding and macromolecular confinement on biochemical reactions in physiological media. *The Journal of biological chemistry* **2001,** *276* (14), 10577-80.
2. Dauty, E.; Verkman, A. S., Molecular crowding reduces to a similar extent the diffusion of small solutes and macromolecules: measurement by fluorescence correlation spectroscopy. *Journal of molecular recognition : JMR* **2004,** *17* (5), 441-7.
3. van den Berg, B.; Ellis, R. J.; Dobson, C. M., Effects of macromolecular crowding on protein folding and aggregation. *The EMBO journal* **1999,** *18* (24), 6927-33.
4. van den Berg, B.; Wain, R.; Dobson, C. M.; Ellis, R. J., Macromolecular crowding perturbs protein refolding kinetics: implications for folding inside the cell. *The EMBO journal* **2000,** *19* (15), 3870-5.
5. Zorrilla, S.; Hink, M. A.; Visser, A. J. W. G.; Lillo, M. P., Translational and rotational motions of proteins in a protein crowded environment. *Biophysical Chemistry* **2007,** *125* (2–3), 298-305.
6. Megan Currie, C. T., Randi Timerman, Robb Welty, Brenden Berry Erin D. Sheets, Ahmed A. Heikal, Multiscale diffusion of a molecular probe in a crowded environment: a concept. *SPIE* **2002,** *Vol. 9584* (Ultrafast Nonlinear Imaging and Spectroscopy III), 16.
7. Ellis, R. J., Protein Misassembly. In *Molecular Aspects of the Stress Response: Chaperones, Membranes and Networks*, Csermely, P.; Vígh, L., Eds. Springer New York: 2007; Vol. 594, pp 1-13.
8. Heikal, A. A., Understanding macromolecular crowding is critical for quantitative cell biology. *SPIE Newsroom* **2015,** *Biomedical Optics & Medical Imaging*.
9. Yu, Q.; Heikal, A. A., Two-photon autofluorescence dynamics imaging reveals sensitivity of intracellular NADH concentration and conformation to cell physiology at the single-cell level. *Journal of Photochemistry and Photobiology B-Biology* **2009,** *95* (1), 46-57.
10. Heikal, A. A., Intracellular coenzymes as natural biomarkers for metabolic activities and mitochondrial anomalies. *Biomarkers in Medicine* **2010,** *4* (2), 241-263.
11. Heikal, A. A., A multiparametric imaging of cellular coenzymes for monitoring metabolic and mitochondrial activities. In *Annual Review in Fluorescence 2010*, D.Geddes, C., Ed. Springer: 2012; Vol. 2010, pp 223-243.
12. Gafni, A.; Brand, L., Fluorescence decay studies of reduced nicotinamide adenine dinucleotide in solution and bound to liver alcohol dehydrogenase. *Biochemistry* **1976,** *15* (15), 3165-3171.
13. Harshad D. Vishwasrao, Q. Y., Kuravi Hewawasam, Ahmed A. Heikal, Polarization Imaging of Cellular Autofluorescence. In *Natural Biomarkers for Cellular Metabolism*
Biology, Techniques, and Applications, Heikal, V. V. G. a. A. A., Ed. USA CRC Press: Boca Raton, FL, 2014; pp 107-136.

14. Yu, Q. Functional imaging of intracellular metaboli cofactors in human normal and cancer breast cells. Pennsylvania State University, 2009.
15. Ying, W., NAD^+/NADH and $NADP^+$/NADPH in cellular functions and cell death: regulation and biological consequences. *Antioxidants & Redox Signaling* **2008,** *10*, 179–206.
16. Alirol, E.; Martinou, J. C., Mitochondria and cancer: is there a morphological connection? *Oncogene* **2006,** *25* (34), 4706-4716.
17. Hammen, P. K.; Allali-Hassani, A.; Hallenga, K.; Hurley, T. D.; Weiner, H., Multiple conformations of NAD and NADH when bound to human cytosolic and mitochondrial aldehyde dehydrogenase. *Biochemistry* **2002,** *41* (22), 7156-7168.
18. Vishwasrao, H. D.; Heikal, A. A.; Kasischke, K. A.; Webb, W. W., Conformational dependence of intracellular NADH on metabolic state revealed by associated fluorescence anisotropy. *The Journal of biological chemistry* **2005,** *280* (26), 25119-26.
19. Lakowicz, J. R., *Principles of fluorescence spectroscopy*. 3rd ed.; Springer: New York, 2006; p xxvi, 954 p.
20. Romashko, D. N.; Marban, E.; O'Rourke, B., Subcellular metabolic transients and mitochondrial redox waves in heart cells. *Proceedings of the National Academy of Sciences of the United States of America* **1998,** *95* (4), 1618-23.
21. Rocheleau, J. V.; Head, W. S.; Piston, D. W., Quantitative NAD(P)H/flavoprotein autofluorescence imaging reveals metabolic mechanisms of pancreatic islet pyruvate response. *J. Biol. Chem.* **2004,** *279*, 31780-7.
22. Biagini, G. A.; Viriyavejakul, P.; O'Neill P, M.; Bray, P. G.; Ward, S. A., Functional characterization and target validation of alternative complex I of Plasmodium falciparum mitochondria. *Antimicrobial agents and chemotherapy* **2006,** *50* (5), 1841-51.
23. Probes for Mitochondria—Section 12.2. https://www.thermofisher.com/us/en/home/references/molecular-probes-the-handbook/probes-for-organelles/probes-for-mitochondria.html (accessed 7-10-2017).
24. O'connor DV, P. D., Time-Correlated Single-Photon Counting. *Academic Press* **1984**.
25. Huang, S.; Heikal, A. A.; Webb, W. W., Two-photon fluorescence spectroscopy and microscopy of NAD(P)H and flavoprotein. *Biophysical journal* **2002,** *82* (5), 2811-2825.
26. Zorrilla, S.; Rivas, G.; Lillo, M. P., Fluorescence anisotropy as a probe to study tracer proteins in crowded solutions. *Journal of molecular recognition : JMR* **2004,** *17* (5), 408-16.
27. Ruzin, S. E., Plant Microtechnique and Microscopy. **1999**, 336.
28. Everett, M., DIC Imaging using Laser Scanning Microscopes (LSM) on Inverted Stands. *Carl Zeiss MicroImaging*, 8.
29. Yu, Q.; Proia, M.; Heikal, A. A., Integrated biophotonics approach for noninvasive and multiscale studies of biomolecular and cellular biophysics. *J. Biomed. Opt.* **2008,** *13* (4), 041315.

30. Vladimir V. Ghukasyan, A. A. H., Natural Biomarkers for Cellular Metabolism: Biology, Techniques, and Applications. **2014,** (Series in Cellular and Clinical Imaging), 408.
31. J. Dijksterhuis, J. N., F. A. Hoekstra, E. A. Golovina, High Viscosity and Anisotropy Characterize the Cytoplasm of Fungal Dormant Stress-Resistant Spores. *Eukaryotic Cell* **2007,** *6* (2), 157-170.
32. Zhou, H. X.; Rivas, G.; Minton, A. P., Macromolecular crowding and confinement: biochemical, biophysical, and potential physiological consequences. *Annual review of biophysics* **2008,** *37*, 375-97.
33. Minton, A. P., Confinement as a determinant of macromolecular structure and reactivity. *Biophys J* **1992,** *63* (4), 1090-1100.
34. Damien Hall, A. P. M., Macromolecular crowding: qualitative and semiquantitative successes, quantitative challenges. *Biochimica et Biophysica Acta* **2003,** *1649* (2), 127– 139.
35. Isabel Pastor, L. P., Cristina Balcells, Eudald Vilaseca, Sergio Madurga, Adriana Isvoran, Marta Cascante, Francesc Mas, Effect of crowding by Dextrans in enzymatic reactions. *Biophysical Chemistry* **2014,** *185*, 8-13.
36. Wang, Y.; Li, C.; Pielak, G. J., Effects of proteins on protein diffusion. *J Am Chem Soc* **2010,** *132* (27), 9392-7.
37. Aumiller, W. M., Jr.; Davis, B.W.; Hatzakis, E.; Keating, C.D, Interactions of macromolecular crowding agents and cosolutes with small-molecule substrates: Effect on horseradish peroxidase activity with two different substrates. *Journal of Physical Chemistry* **2014,** *118*, 10624–10632.
38. Alexander Christiansen, Q. W., Antonios Samiotakis, Margaret S. Cheung, and Pernilla Wittung-Stafshede, Factors Defining Effects of Macromolecular Crowding on Protein Stability: An in Vitro/in Silico Case Study Using Cytochrome c†. *Biochemistry* **2010,** *2010* (49), 6519-6530.
39. Samiotakis, A.; Wittung-Stafshede, P.; Cheung, M. S., Folding, Stability and Shape of Proteins in Crowded Environments: Experimental and Computational Approaches. *International Journal of Molecular Sciences* **2009,** *10*, 572-588.
40. Monette, R.; Small, D. L.; Mealing, G.; Morley, P., A fluorescence confocal assay to assess neuronal viability in brain slices. *Brain Research Protocols* **1998,** *2* (2), 99-108.
41. L F Barros, T. K., R Sabirov, S Morishima, J Castro, C X Bittner, E Maeno, Y Ando-Akatsuka, and Y Okada, Apoptotic and necrotic blebs in epithelial cells display similar neck diameters but different kinase dependency. *nature* **2003,** *10*, 687–697.
42. Nianyu Li, K. R., Gretchen Lawler, Jennie Sturgis, Bartek Rajwa, J. Andres Melendez, and J. Paul Robinson, Mitochondrial Complex I Inhibitor Rotenone Induces Apoptosis through Enhancing Mitochondrial Reactive Oxygen Species Production. *The Journal of biological chemistry* **2002,** *278*, 8516-8525.

43. Barrientos, A.; Fontanesi, F.; Díaz, F., Evaluation of the Mitochondrial Respiratory Chain and Oxidative Phosphorylation System using Polarography and Spectrophotometric Enzyme Assays. *Current protocols in human genetics / editorial board, Jonathan L. Haines ... [et al.]* **2009,** *Chapter*, Unit19.3.
44. Sandeep Chakraborty, F.-S. N., Jin-Wu Tsai, Artashes Karmenyan, Arthur Chiou, Quantification of the Metabolic State in Cell-Model of Parkinson's Disease by Fluorescence Lifetime Imaging Microscopy. *Scientific Reports* **2016**.
45. Koch-Nolte, F.; Fischer, S.; Haag, F.; Ziegler, M., Compartmentation of NAD+-dependent signalling. *FEBS Letters* **2011,** *585* (11), 1651-1656.
46. Wright, B. K.; Andrews, L. M.; Jones, M. R.; Stringari, C.; Digman, M. A.; Gratton, E., Phasor-FLIM analysis of NADH distribution and localization in the nucleus of live progenitor myoblast cells. *Microscopy research and technique* **2012,** *75* (12), 1717-1722.

Appendix 1.1

Table 1.1: Time-resolved fluorescence lifetime parameters (heterogeneous crowding)

Environment: [NADH]:[LDH]	α_1	τ_1 (ns)	α_2	τ_2 (ns)	α_3	τ_3 (ns)	f_b (%)	K_d (μM)
Ficoll-70: (200g/L)								0.103
1:1	0.81	1.085	0.191	2.824	--	--	1	±
2:1	0.79	1.065	0.208	2.603	--	--	1	0.03063
4:1	0.59	0.433	0.352	1.147	0.061	2.957	0.69	
5:1	0.51	0.561	0.439	1.416	0.048	3.369	0.72	
8:1	0.51	0.579	0.442	1.411	0.051	3.289	0.72	
16:1	0.71	0.365	0.262	0.832	0.024	3.150	0.09	
32:1	0.69	0.367	0.275	0.875	0.037	2.710	0.13	
1:0	0.68	0.343	0.31	0.695	0.009	3.609	0	
Ficoll-70: (400g/L)								0.1246
1:1	0.63	2.02	0.289	1.731	0.079	4.232	1	±
2:1	0.60	0.926	0.337	1.683	0.065	3.812	1	0.03444
4:1	0.58	0.536	0.355	1.376	0.049	3.377	0.65	
5:1	0.59	0.51	0.37	1.356	0.041	3.538	0.66	
8:1	0.64	0.461	0.317	1.186	0.046	3.082	0.61	
16:1	0.67	0.414	0.289	1.020	0.039	2.849	0.10	
32:1	0.71	0.4	0.262	0.884	0.025	2.734	0.04	
1:0	0.70	0.383	0.281	0.795	0.017	2.678	0	
Ficoll-400 (200g/L)								0.0674
1:1	0.84	1.08	0.164	2.91	--	--	1	±
2:1	0.83	1.05	0.175	2.86	--	--	1	0.01717
4:1	0.60	0.461	0.365	1.30	0.043	3.24	0.69	
5:1	0.53	0.564	0.428	1.42	0.044	3.76	0.72	
8:1	0.61	0.449	0.354	1.30	0.040	3.43	0.68	
16:1	0.70	0.384	0.268	1.06	0.036	2.96	0.59	
32:1	0.73	0.349	0.246	0.766	0.022	2.35	0.09	
1:0	0.65	0.331	0.325	0.575	0.022	1.49	0	

Environment: [NADH]:[LDH]	α_1	τ_1 (ns)	α_2	τ_2 (ns)	α_3	τ_3 (ns)	f_b (%)	K_d (μM)
Dextran-6: (200g/L)								0.056
1:1	0.73	1.03	0.269	2.16	--	--	1	±
2:1	0.70	1.01	0.298	2.04	--	--	1	0.0124
4:1	0.65	0.685	0.350	1.82	--	--	0.99	
5:1	0.54	0.582	0.391	1.43	0.0066	2.56	0.64	
8:1	0.60	0.493	0.348	1.31	0.0056	2.53	0.61	
16:1	0.70	0.430	0.245	1.04	0.0054	2.30	0.47	
32:1	0.71	0.403	0.244	0.828	0.0049	2.08	0.42	
1:0	0.69	0.354	0.297	0.673	0.0014	2.359	0	
Dextran-6 (300g/L)								0.057
1:1	0.75	1.02	0.251	2.24	--	--	1	±
2:1	0.71	0.984	0.293	2.11	--	--	1	0.0097
4:1	0.52	0.662	0.414	1.50	0.069	2.698	0.69	
5:1	0.50	0.642	0.434	1.45	0.071	2.586	0.71	
8:1	0.61	0.492	0.339	1.28	0.055	2.649	0.64	
16:1	0.68	0.436	0.279	1.07	0.045	2.626	0.56	
32:1	0.73	0.426	0.229	0.906	0.037	2.338	0.45	
1:0	0.67	0.388	0.314	0.715	0.018	2.289	0	
Dextran-70: (200g/L)								0.092
1:1	0.70	1.02	0.302	1.997	--	--	1	±
2:1	0.69	0.964	0.311	1.996	--	--	1	0.0157
4:1	0.54	0.679	0.385	1.506	0.071	2.391	0.69	
5:1	0.67	0.446	0.259	1.225	0.055	2.208	0.72	
8:1	0.70	0.444	0.239	1.119	0.059	2.117	0.72	
16:1	0.74	0.440	0.202	1.009	0.050	2.021	0.09	
32:1	0.74	0.411	0.22	0.687	0.045	1.320	0.13	
1:0	0.75	0.406	0.229	0.758	0.027	1.509	0	

Environment: [NADH]:[LDH]	α_1	τ_1 (ns)	α_2	τ_2 (ns)	α_3	τ_3 (ns)	f_b (%)	K_d (μM)
Dextran-70: (300g/L)								0.097
1:1	0.76	0.960	0.244	2.653	--	--	1	±
2:1	0.65	0.910	0.354	1.912	--	--	1	0.0226
4:1	0.54	0.642	0.389	1.493	0.069	2.400	0.66	
5:1	0.56	0.511	0.384	1.299	0.054	2.687	0.66	
8:1	0.68	0.425	0.270	0.854	0.05	1.992	0.49	
16:1	0.68	0.471	0.266	1.189	0.058	2.217	0.54	
32:1	0.68	0.406	0.276	0.749	0.048	1.709	0.06	
1:0	0.66	0.397	0.310	0.727	0.029	1.6451	0	
Dextran-150: (200g/L)								0.1031
1:1	0.75	1.049	0.249	2.199	--	--	1	±
2:1	0.71	0.992	0.293	2.096	--	--	1	0.02268
4:1	0.49	0.63	0.444	1.454	0.064	2.547	0.72	
5:1	0.54	0.552	0.398	1.367	0.063	2.632	0.70	
8:1	0.66	0.471	0.293	1.261	0.05	2.512	0.61	
16:1	0.71	0.403	0.238	0.846	0.054	2.048	0.18	
32:1	0.75	0.415	0.211	0.909	0.038	2.277	0.14	
1:0	0.70	0.381	0.295	0.680	1E-3	--	0	
Dextran-150: (300g/L)								0.1246
1:1	0.63	2.02	0.289	1.731	0.079	4.232	1	±
2:1	0.60	0.926	0.337	1.683	0.065	3.812	1	0.03444
4:1	0.58	0.536	0.355	1.376	0.049	3.377	0.65	
5:1	0.59	0.51	0.37	1.356	0.041	3.538	0.66	
8:1	0.64	0.461	0.317	1.186	0.046	3.082	0.61	
16:1	0.67	0.414	0.289	1.020	0.039	2.849	0.10	
32:1	0.71	0.4	0.262	0.884	0.025	2.734	0.04	
1:0	0.70	0.383	0.281	0.795	0.017	2.678	0	

Appendix 1.2

Table 1.2: Time-resolved fluorescence anisotropy parameters (heterogeneous crowding)

Environment: [NADH]:[LDH]	β_1	φ_1 (ns)	β_2	φ_2 (ns)	r_0	f_β (%)	K_d (μM)
Ficoll-70: (200g/L)							0.106
1:1	0.17	0.008	0.47	39.14	0.45	0.97	±
2:1	0.06	0.04	0.48	32.92	0.41	0.92	0.003
4:1	0.29	0.13	0.45	37.37	0.39	0.74	
5:1	0.25	0.11	0.57	16.19	0.39	0.57	
8:1	0.27	0.14	0.51	15.67	0.36	0.53	
16:1	0.22	0.22	0.57	8.08	0.34	0.33	
32:1	0.27	0.29	0.57	5.70	0.34	0.22	
1:0	0.18	0.12	0.16	3.3	0.34	0	
Ficoll-70: (400g/L)							0.112
1:1	0.43	0.01	0.47	118.60	0.47	0.91	±
2:1	0.24	0.08	0.46	59.72	0.43	0.91	0.019
4:1	0.29	0.19	0.49	23.64	0.42	0.64	
5:1	0.26	0.21	0.52	13.04	0.39	0.58	
8:1	0.25	0.53	0.57	6.42	0.40	0.43	
16:1	0.25	0.36	0.57	5.10	0.40	0.40	
32:1	0.21	0.36	0.57	4.64	0.38	0.37	
1:0	0.14	0.16	0.23	5.45	0.38	0	
Ficoll-400: (200g/l)							0.050
1:1	0.57	0.02	0.45	63.88	0.47	0.99	±
2:1	0.56	0.01	0.45	60.88	0.46	0.98	0.0049
4:1	41	0.15	0.42	152.5	0.41	0.79	
5:1	0.37	0.08	0.44	49.86	0.42	0.85	
8:1	0.34	0.18	0.43	47.83	0.40	0.74	
16:1	0.38	0.19	0.42	29.19	0.38	0.52	
32:1	0.38	0.22	0.37	34.00	0.37	0.35	
1:0	0.27	0.19	0.10	7.1E107	0.37	0	

Environment: [NADH]:[LDH]	β_1	φ_1 (ns)	β_2	φ_2 (ns)	r_0	f_b (%)	K_d (μM)
Dextran-6: (200g/L)							0.0357
1:1	– –	– –	0.465	48.9	0.45	1	±
2:1	– –	– –	0.461	57.54	0.45	1	0.0057
4:1	0.077	5.87E-4	0.458	72.62	0.44	0.97	
5:1	0.195	0.059	0.4679	57.54	0.43	0.93	
8:1	0.37	0.09	0.483	41.86	0.43	0.80	
16:1	0.343	0.156	0.471	31.15	0.40	0.57	
32:1	0.24	0.476	0.42	31.72	0.32	0.41	
1:0	0.25	0.419	0.064	1.05E95	0.37	0	
Dextran-6: (300g/L)							0.038
1:1	– –	– –	0.455	52.00	0.453	1	±
2:1	0.278	0.013	0.454	67.25	0.445	0.99	0.00393
4:1	0.444	0.033	0.457	61.50	0.455	0.93	
5:1	0.3638	0.07	0.488	39.46	0.457	0.87	
8:1	0.318	0.092	0.535	24.15	0.448	0.71	
16:1	0.258	0.325	0.46	20.30	0.375	0.58	
32:1	0.257	0.40	0.46	15.34	0.367	0.45	
1:0	0.208	0.194	0.126	1.88	0.42	0	
Dextran-70: (200g/L)							0.0597
1:1	– –	– –	0.465	68.89	0.455	1	±
2:1	– –	– –	0.464	84.71	0.444	1	0.01624
4:1	0.214	0.011	0.472	68.9	0.448	0.94	
5:1	0.563	0.044	0.45	174.9	0.462	0.94	
8:1	0.308	0.210	0.449	57.56	0.40	0.63	
16:1	0.351	0.304	0.379	1.8E19	0.393	0.50	
32:1	0.231	0.446	0.535	18.18	0.322	0.11	
1:0	0.307	0.257	0.0893	1.7E110	0.421	0	

Environment: [NADH]:[LDH]	β_1	φ_1 (ns)	β_2	φ_2 (ns)	r_0	f_b (%)	K_d (μM)
Dextran-70: (300g/L)							0.0596
1:1	--	--	0.465	288.5	0.47	1	±
2:1	--	--	0.452	37.15	0.449	1	0.0165
4:1	0.29	0.19	0.49	23.64	0.429	0.97	
5:1	0.346	0.15	0.57	3.5E20	0.44	0.50	
8:1	0.311	0.27	0.40	6.42	0.399	0.76	
16:1	0.343	0.21	0.57	21.03	0.44	0.45	
32:1	0.353	0.306	0.57	16.00	0.446	0.37	
1:0	0.224	0.303	0.135	2.5E99	0.40	0	
Dextran-150: (200g/L)							0.064
1:1	--	--	0.45	59.9	0.45	1	±
2:1	--	--	0.46	55.27	0.46	1	0.0129
4:1	0.377	0.33	0.48	42.10	0.45	0.91	
5:1	0.34	0.079	0.512	21.03	0.46	0.84	
8:1	0.32	0.127	0.57	13.86	0.43	0.55	
16:1	0.335	0.227	0.57	10.34	0.42	0.36	
32:1	0.356	0.227	0.57	8.94	0.43	0.36	
1:0	0.295	0.376	0.06	55.61	0.41	0	
Dextran-150: (300g/L)							0.052
1:1	--	--	0.453	34.62	0.45	1	±
2:1	0.016	0.035	0.518	16.81	0.42	0.85	0.01051
4:1	0.366	0.065	0.475	20.88	0.44	0.85	
5:1	0.30	0.106	0.529	15.79	0.43	0.69	
8:1	0.338	0.143	0.516	10.48	0.43	0.62	
16:1	0.296	0.204	0.540	10.47	0.41	0.50	
32:1	0.419	0.277	0.367	6.67	0.42	0.56	
1:0	0.220	0.265	0.179	5.94	0.42	0	